A unified rodent atlas reveals the cellular complexity and evolutionary divergence of the dorsal vagal complex

Cecilia Hes[1,2], Abigail J. Tomlinson[3], Lieke Michielsen[4], Hunter J. Murdoch[1,5], Fatemeh Soltani[1,2], Maia Kokoeva[1,5,6], Paul V. Sabatini[1,2,6]*

***Corresponding author**: paul.sabatini@mcgill.ca

Author affiliations:

1. McGill University Health Centre Research Institute, Montreal QC, Canada
2. Division of Experimental Medicine, Department of Medicine, McGill University, Montreal QC, Canada
3. Department of Internal Medicine, University of Michigan, Ann Arbor MI, USA
4. Department of Human Genetics, Leiden University Medical Center, Leiden, The Netherlands
5. Integrated Program in Neuroscience, McGill University, Montreal QC, Canada
6. Division of Endocrinology, Department of Medicine, McGill University, Montreal QC, Canada

Keywords:

DVC, area postrema, nucleus of the solitary tract, cell atlas, GLP1, PDGFRA, CCK, TH

Abstract

The dorsal vagal complex (DVC) is a region in the brainstem comprised of an intricate network of specialized cells responsible for sensing and propagating many appetite-related cues. Understanding the dynamics controlling appetite requires deeply exploring the cell types and transitory states harbored in this brain site. We generated a multi-species DVC cell atlas using single nuclei RNAseq (sn-RNAseq), thorough curation and harmonization of mouse and rat data which includes >180,000 cells and 123 cell identities at 5 granularities of cellular resolution. We report unique DVC features such as Kcnj3 expression in Ca^{+}-permeable astrocytes as well as new cell populations like neurons co-expressing *Th* and *Cck*, and a leptin receptor-expressing neuron population in the rat area postrema which is marked by expression of the progenitor marker, *Pdgfra*. In summary, our findings suggest there are distinct cellular populations specific to the DVC compared to other brain sites and our comprehensive atlas is a valuable tool for the study of this metabolic center.

Introduction

Regulating appetite in response to changing environmental conditions to maintain energy balance requires the intricate interplay of multiple organs. Within the central nervous system, an incredible diversity of discrete brain regions and cell types control appetite(*1*). More specifically, the dorsal vagal complex (DVC) of the brainstem, comprising the area postrema (AP), nucleus of the solitary tract (NTS) and dorsal motor nucleus of the vagus (DMV), acts as a key nexus point for metabolic signals, evidenced by the dense expression of many relevant hormone receptors(*2*). Separately, the DVC also serves as the primary site of gut-based signals via vagal afferents(*3-5*). Functionally, the DVC was long considered a site promoting meal termination(*6*) but growing evidence suggests the DVC also regulates long-term energy balance(*7, 8*).

Much of the interest in DVC neurons' role in appetite and energy balance stems from their role as therapeutic targets for obesity and anorexia in cancer cachexia(*9, 10*). For many years, most pharmacotherapies failed to produce efficacious and long-lasting weight loss in obesity and increase appetite in cancer cachexia(*11*). More recently however, the glucagon-like peptide 1 receptor (GLP1R) agonists are eclipsing the weight loss achieved by previous generations of therapeutics(*12*). While expressed across the central nervous system, GLP1R expression is particularly enriched in DVC neurons(*13*) and it is the DVC that mediates many of the effects of GLP1R agonists(*14*). Separately, an emerging strategy for treating cancer cachexia is inhibiting growth differentiation factor 15 (GDF15) signaling in the DVC by blocking the action of GDNF Family Receptor Alpha Like (GFRAL)(*15*), the receptor for GDF15(*16*). Given the clinical significance of the DVC for this spectrum of conditions, understanding the

59 molecular heterogeneity and function of this region is essential to understand appetite
60 regulation without major side effects.
61
62 Traditionally, identification and ensuing study of DVC cell types was limited to known
63 neurotransmitter and receptor-expressing cell types. For instance, the cholecystokinin and
64 monoamine-expressing cells, demarcated by tyrosine hydroxylase (*Th*) expression, were
65 previously shown to be non-overlapping cell populations with unique roles in appetite
66 suppression(*17*). More recently, the advent of single-cell mRNA sequencing approaches made
67 unbiased molecular censuses of heterogenous populations possible. Such studies focusing
68 on the mouse have revealed the complexity of the mouse DVC, comprised of dozens of
69 transcriptionally distinct cell types(*2, 18, 19*). Moving forward, unifying information from multiple
70 single-nuclei RNA sequencing (snRNA-seq) datasets of the DVC into a reference atlas is
71 needed to more fully understand the cells within the DVC and generate a common and scalable
72 classification for cell classes. Such a reference atlas is also needed to contrast the cell types
73 found within the mouse to other research models, including the rat, which are prominent
74 models for DVC biology(*2, 20*).
75
76 To address this, we generated a comprehensive snRNA-seq based atlas of the mouse and rat
77 DVC. This atlas features mouse and rat labelled cells with increasing granularity and an
78 accompanying computational toolbox including the mouse and rodent atlas label transfer
79 environment using treeArches. The mouse DVC atlas reveals a higher degree of cellular
80 complexity than previously appreciated. The cellular census of the rat DVC exhibits many
81 similarities to the mouse but also rat-specific cells including a novel population of leptin
82 receptor and *Pdgfra*-expressing neurons localized to the AP. We then used this unified atlas
83 to uncover the cell types that transcriptionally respond to meal consumption which may hold
84 the potential of suppressing appetite without gastrointestinal side effects.
85

86 **Results**

87 <u>The murine dorsal vagal complex cell classes</u>
88 To generate a snRNA-seq atlas of the mouse DVC, we isolated the DVC from 30 adult
89 C57BL/6J mice and subjected them to 10X Genomics-based snRNA barcoding and
90 sequencing (Fig.1A). From the CellRanger pre-processing pipeline(*21*) we obtained 110,167
91 cells of which 99,740 were retained after processing. Cell identities were initially mapped to 5
92 databases from different brain regions and then curated manually using 473 cell identity
93 markers (Tables S1-S2). We distinguished clusters of neurons and glial, vascular and
94 connective tissue cells, a first layer of cell identity (Fig.1B; Table S3). We further describe a
95 second layer of cellular resolution, which are subgroups of the first layer that contain the cell
96 classes (Fig.1C; Table S3).

97
98 Among the ten neuronal cell classes identified at layer 2 resolution, we found two major groups
99 which we called 'magnaclass1' and 'magnaclass2' (**Fig.S1**). Magnaclass1 neurons
100 predominately express genes required for inhibitory neurotransmission (e.g. *Gad1*, *Gad2*) and
101 share transcriptomic markers with the Sall3-class of neurons, whereas magnaclass2 neurons
102 express mostly excitatory transcripts (e.g. the glutamate transporter VGLUT2) also found in the
103 Lhx2-class and monoamine-class (**Fig.1D-E**; **Fig.S1**). However, as described in other brain
104 areas(*22, 23*), evidence of co-transmission/co-release of multiple primary neurotransmitters
105 was found in at least 55% of neurons regardless of their cell class (**Fig.1D-E**; **Table S4**). We
106 also identified 8 transcriptionally distinct neural classes in addition to the magnaclasses. The
107 Golli-class expresses myelin-associated genes such as *Mag* and *Mog*(*24-26*) (**Fig.1D**; **Table**
108 **S5**). Moreover, we describe the corelautus-class (Latin: 'washed nucleus'), distinguished by a
109 large number of downregulated genes in the nuclei compared to other neuronal classes, and
110 a class with genes normally upregulated in astrocytes (e.g. *Slc6a11*) and related to clearance
111 and uptake of glutamate, gamma-aminobutyric acid (GABA), Ca^{+} and bicarbonate (*27, 28*),
112 which we named 'pH-related class' (**Table S5**). When interrogating snRNA-seq data from the
113 hypothalamus(*29*) (**Fig.S2**), another brain site important for energy balance, we could not find
114 clusters sharing all markers with our neuronal classes, indicating DVC-specific neuronal
115 programs (**Fig.S2C**).
116
117 <u>The murine DVC cells at their highest resolution</u>
118 To better define the heterogeneity of the mouse DVC, we further assigned a clustering-based
119 third layer of cellular resolution resulting in fifty cell identities, of which 15 are non-neuronal
120 (**Fig.2A**). At this resolution we differentiated between two major groups of astrocytes.
121 Differential expression in synapse-related factors revealed a group of highly excitable
122 astrocytes with high expression of the inwardly rectifying GIRK1 (*Kcnj3*) channel(*30*) and lack
123 of expression of the AMPAr subunit GluA2 (*Gria2*), additionally rendering them K^{+}/Na^{+}/Ca^{+}-
124 permeable(*31, 32*) (**Fig.2B**). We speculate these astrocytes are specific to the DVC as we could
125 not find Kcnj3+; Gria2- astrocytes in the hypothalamus, cortex or hippocampus(*29, 33*)
126 (**Fig.S2D**; **Fig.S3**). In addition, we distinguished a spectrum of DVC mature oligodendrocytes,
127 including a group resembling the intermediate oligodendrocytes described in the other brain
128 sites that decrease in number with age(*34*) (**Fig.2C**). This gradient of expression of markers
129 including *Fyn*, *Opalin* and *Anln* in oligodendrocytes (**Fig.2C**), do not respond to a
130 developmental trajectory (**Fig.S4**). Although 'myelinating-intermediate' and 'myelinating'
131 oligodendrocytes include cells with overlapping gene expression programs, there is no
132 evidence that each oligodendrocyte will follow a single trajectory (**Fig.S4**). Furthermore, to
133 properly separate some cell identities, we performed sub-clustering in three DVC clusters (i.e.
134 clusters 23, 26 and 27) (**Fig.S5A**). This permitted us to label pre-myelinating oligodendrocytes,

135 endothelial and mural cells, and distinguish two fibroblast sub-types (**Fig.S5**). One of these
136 subtypes expresses high *Stk39* previously described in fibroblast stress-response(*35*) and so
137 was termed 's-fibroblasts' for stress-associated fibroblasts (**Fig.S5B**), which we failed to detect
138 in the hypothalamus (**Fig.S2E**). Additionally, there was no evidence of reactive microglia as we
139 mapped minimal levels of the activation genes *Cxcl10*, *Cd5*, *Cxcl9* and *Zbp1*(*36*), therefore we
140 posit that our DVC microglial cells are in a basal state (**Fig.S6**). We also obtained the DVC gene
141 expression markers of the main cell types in the central nervous system and neurons (**Fig.2D**).
142
143 To more thoroughly classify DVC neural types, we subset and re-clustered the 10 neural
144 classes from layer 2 which resulted in 35 neuronal identities as a third layer of granularity
145 (**Fig.3A**; **Table S5**). These identities include 'preganglionic' or *Chat*-expressing neurons and a
146 large number of neurons with unspecific markers which we called 'mixed neurons' (**Table S5**).
147 A mixed neurons-like group of cells was previously described in the murine hypothalamus(*37*).
148 Additionally, we split the monoamine-class into four layer-3 cell identities (i.e. M0, M1, M2 and
149 M3) with specific cell markers (**Fig.3B**; **Table S5**). M0 and M1 neurons express genes for
150 enzymes synthesizing norepinephrine and serotonin, but M0 expresses minimal levels of the
151 transporter VMAT2 (*Slc18a2*) (**Fig.3C**; **Table S5**). Due to the low proportion of cells expressing
152 *Th* and *Tph2* in M2 and M3 neurons, we consider them monoamine-modulators as they seem
153 to synthesize trace amines (**Fig.3C**; **Table S5**). Of note, the receptor for GDF15, GFRAL, is
154 expressed heavily by a subset of M0 neurons, some of which co-express the calcium sensing
155 receptor (*Casr*) gene (**Fig.3C**).
156
157 We named 'GLP1' a neuronal cluster with high expression of the pre-proglucagon gene (*Gcg*)
158 (**Fig.3D**; **Table S5**), which also expresses high levels of both the prolactin and leptin
159 receptors(*38*) (**Fig.3E**). Additionally, these cells have the highest proportion of DVC neuronal
160 co-expression of glutamate and GABA related genes (**Fig.3F**).
161
162 In our analysis we found a subset of monoaminergic neurons that express the cholecystokinin
163 (*Cck*) gene (**Fig.4A**). While the *Cck* and *Th*-expressing DVC neurons are considered to be non-
164 overlapping cell types with distinct physiologies(*39*), we confirmed co-expression of *Th* and
165 *Cck* results by *in-situ* hybridization (**Fig.4B**). The majority of this overlap occurs in cells
166 belonging to the COE-Atp10a and monoamine class (i.e. M0, M3) cell identities (**Fig.4A**).
167
168 <u>The murine DVC cell atlas</u>
169 To generate a comprehensive murine DVC database from multiple datasets, we utilized
170 treeArches(*40*) to harmonize our snRNA-seq DVC labels with that from a publication by Ludwig
171 and collaborators (i.e. the 'Ludwig dataset')(*2*) (**Fig.5A-B**). After building our initial cell hierarchy
172 (**Fig.S7**), we integrated our dataset with the Ludwig dataset, giving a total of 171,868 cells

173 (Fig.5B). Next, the labeled cell identities from the Ludwig dataset(*2*) were incorporated into our
174 tree based on the similarity between the transcriptomic programs of our labeled identities and
175 the Ludwig-labeled identities using progressive learning through scHPL(*41*) (Fig.5A). Some of
176 the Ludwig dataset identities failed to be incorporated into our tree, like the oligodendrocyte
177 precursor cells (OPCs), which contain a mix of OPCs and pre-myelinating oligodendrocytes
178 (Fig.S8A). The mix of cell programs makes it impossible for treeArches to correctly add one
179 branch of the Ludwig OPCs to the tree as ideally it would be added as a subpopulation of both
180 the OPCs and pre-myelinating oligodendrocytes, which is not biologically possible. The
181 resultant murine hierarchy has a fourth layer of cellular resolution as some of Ludwig identities,
182 mainly neurons, are subgroups of our cell identities (Fig.S8B).
183
184 We confirmed the validity of our cell hierarchy using three methods. First, by using the learned
185 model to predict the labels of the cells we used to develop them (i.e. this study and the Ludwig
186 dataset), for which we obtained highly concordant cell labeling (Fig.5C). Secondly, we used
187 the learned model to predict the labels of another publicly available dataset from Dowsett and
188 collaborators (i.e. the 'Dowsett dataset')(*18*) (Fig.5D). Using this approach, we were able to
189 successfully label 95% of these cells at high resolution (i.e. layer 3 or 4 of cell identity
190 granularity); further validating our combined DVC labels. Finally, we manually mapped the
191 marker genes from Ludwig(*2*) and Dowsett(*18*) neuronal clusters in our dataset and confirmed
192 the sub-groups of neurons among our identities pointed out by treeArches (Fig.S8B).
193
194 <u>An integrated rodent DVC cell hierarchy</u>
195 To identify rat DVC cell clusters and subclusters and contrast these with the mouse DVC atlas,
196 we generated a *de novo* ad libitum-fed rat dataset (cells n=12,167) (Fig.6A) and labeled it by
197 mapping the top 5 gene expression markers of each of our murine layer-3 cell identities (Table
198 S6). After manual curation at three granularities (Fig.6B-C; Table S7), we obtained 52 DVC rat
199 identities at high cellular resolution (Fig.6C) including a small group of 'unspecific' cells (n=35)
200 that we could not confidently label because its top gene expression markers have unknown
201 functions and none of our known identities' genes clearly marked this population (Fig.6B-C;
202 Table S6).
203
204 We established 10, layer-3 neuronal identities not previously found in the murine data (Fig.6C;
205 Fig.S9A; Table S7). Notably, two of those did not belong to any of the existing murine neuronal
206 classes (i.e. layer-2 of cellular granularity), therefore we created two new layer-2 classes
207 (Fig.6B). One of these, the immunity-related neurons, have high cystatin C, *Inpp5d* and *Csf1r*
208 expression, genes commonly associated with immunity-related processes in microglia and
209 with immunomodulation in cancer(*42-44*) (Fig.7; Table S7). The second neural class identified
210 in rat but not mouse DVC were the 'Pdgfra neurons' (Fig.7). These neurons express *Pdgfra*,

211 *Arhgap31* and *Itga9*, known markers for progenitor cells for which we named this cell class
212 'ortus-akin' (Latin: 'origin') because they are similar to cells giving origin to other cells(*45*)
213 (Fig.7A; Table S7). Interestingly, this neuronal class not only expressed *Pdgfra*, but also other
214 OPC signature genes (Fig.7A). Mapping the expression levels of metabolic-associated
215 receptors revealed that both immunity-akin and ortus-akin express GFRAL, prolactin receptor
216 and leptin receptor (Fig.7B), although they seem to have a varied neurotransmitter profile
217 (Fig.S9B). To confirm the presence of *Pdgfra*-expressing neurons in the rat DVC, we performed
218 immunostaining in the mouse and rat brainstem. Within the mouse, we found PDGFRA-
219 immunoreactivity(IR) in the two morphologically distinct cells; matching OPC and blood vessel-
220 associated fibroblast morphologies(Fig.7C). However, within the rat, we identified PDGFRA-IR
221 in cells with three morphologies, one of which resembled neurons with an enlarged cell body
222 and protruding cellular processes (Fig.7C). To determine if these PDGFRA-IR cells were
223 neurons, we co-stained with the neural marker, HuC/D and noted several PDGFRA and HuC/D
224 copositive cells (Fig.7D); confirming our sequencing data that a PDGFRA-expressing neural
225 class exists in the rat DVC and localizing these cells to the area postrema.
226
227 To construct an integrated rodent DVC cell atlas, we incorporated the labeled rat dataset into
228 our hierarchy using treeArches(*40*) (Fig.8). The rodent data was projected onto the mouse
229 datasets (Fig.8A) and the 42 high resolution rat cell identities were appended to the tree
230 (Fig.8B; Fig.S10). The final hierarchy has 123 labels of which 99 are high resolution according
231 to our cellular granularity (i.e. layers 3 to 5) (Fig.8B). In addition it has 20 layer-2 identities and
232 7 cell identities that are novel from the rat dataset (Fig.8B).
233
234 <u>*Hcrt* and *Agrp* expression in the DVC</u>
235 Since *Agrp* has been described to be expressed in the DVC(*46*), we mapped this and other
236 neuropeptide genes in DVC neurons. Surprisingly, we found *Hcrt* and *Agrp* mRNA in neurons
237 in our dataset (Fig.S11A). We then performed *in-situ* hybridizations for these transcripts in both
238 the mouse hypothalamus and DVC. While both *Hcrt* and *Agrp* were readily detectable in the
239 hypothalamus, we failed to observe signal within the DVC (Fig.S11B). Since we also found
240 expression of *Hcrt* and *Agrp* in neurons of the Dowsett and Ludwig datasets(*2, 18*) (Fig.S11C),
241 we then mapped the sequenced reads from these transcripts and confirmed that most of them
242 mapped to intronic and non-coding regions of these genes (Fig.S11D). Furthermore, our rat
243 DVC dataset was pre-processed excluding introns from the reads mapping, and the *Hcrt* and
244 *Agrp* expression levels observed is minimal (Fig.S11E), which is in agreement with the non-
245 coding location of the reads. These data explain absence of signal from our *in-situ*
246 hybridizations and suggests DVC cells do not produce HCRT or AGRP neuropeptides.
247

248 Meal-related transcriptional programs in the murine DVC
249 As the DVC acts as a primary node for meal-related signals(*47*), we wanted to define which of
250 our cell identities responded to meal consumption and thus performed differential gene
251 expression analysis between DVC cell types from mice that were euthanized under fasting
252 conditions, with ad libitum access to food or two hours post-refeeding following an overnight
253 fast (Fig.1A; Fig.9). This analysis revealed widespread transcriptional changes across nearly
254 every neural cell identity, the exceptions being corelautus, Golli class and pH classes (Fig.9A).
255 Additionally, the size of the transcriptional changes were relatively small, with approximately
256 90% of the differentially expressed genes having increases or decreases between 0.5 and 1.0
257 log2 fold-change, with only ~10% of the gene changes being ≥1 log2 fold-change between
258 conditions (Fig.9A). Of the responding neurons, magnaclasses 1 and 2, which represent large
259 populations of predominately inhibitory and excitatory neurons (Fig.S1), showed the greatest
260 number of differentially expressed genes following refeeding for both comparisons refed
261 versus fasting, and refed versus ad libitum food access (Fig.9A). To understand how refeeding
262 transcriptionally alters inhibitory compared with excitatory DVC neurons, we compared
263 differentially expressed genes between these two classes across conditions. Intriguingly,
264 despite being in transcriptionally distinct classes, we found meal consumption altered many of
265 the same genes (Fig.9B-D), suggesting these cells may be receiving similar postprandial
266 signals which are propagated via these cells in unique manners. This is supported by the
267 similar receptor expression profile of magnaclass 1 and 2 (Fig.S12). One notable exception is
268 *Cckbr* which is upregulated in magnaclass 2 and downregulated in magnaclass 1 in refeeding
269 when compared with ad libitum fed mice, while in refed versus fasted mice (Table S9). We also
270 note that oligodendrocytes contained the highest number of differentially expressed genes in
271 refeeding (Fig.9A), however the roles of oligodendrocytes in refeeding responses within the
272 DVC have yet to be determined and the biologic significance of these changes are presently
273 unclear.
274
275 **Discussion**
276 The recent success of DVC-based therapies(*12, 48*) have moved DVC biology to the forefront
277 of weight control therapies and there is now clear clinical impetus to fully define DVC cell types
278 and their functions. Previous studies detailing DVC cell types describe a high degree of
279 heterogeneity(*2, 18, 19*), however, these studies lacked an in-depth analysis of
280 neurotransmitter profiles of neurons, any cross-species evaluation of DVC cell types, or an
281 analysis of how meal consumption transcriptionally regulates these cells. We therefore
282 developed *de novo* mouse and rat DVC cell atlases to address these points.
283

284 To more fully describe the cellular complexity within the DVC, we combined a pipeline of cell
285 label transfer using brain existing published datasets and thorough curation of cell identities,
286 which resulted in a 4-layer mouse cell hierarchy and a 5-layer rodent cell hierarchy of the DVC.
287 Within this hierarchy we found several unique features of DVC glial cells. First, we found highly
288 excitable Ca^+-permeable astrocytes in the DVC in which *Gfap* is almost exclusively expressed
289 and they coexpress *Kcnj3* (GIRK1 potassium channel). These cells largely lack *Gria2*,
290 consistent with findings in Bergmann glial cells in which colocalization of *Gria2* and GFAP was
291 found to alter neuron-glial interactions(*49*). Comparing Ca^+-permeable DVC astrocytes to
292 hypothalamic astrocytes(*29*), we found the same expression pattern with minimal overlap
293 between *Gria2* and *Gfap.* However, DVC astrocytes seem to have some unique properties
294 when compared with hypothalamic, cortical and hippocampal astrocytes. Principally DVC
295 astrocytes express the GIRK1 channel, likely rendering them more excitable. Additionally,
296 while we identified hypothalamic fibroblasts which express high *Aldh1a1* similar to the DVC p-
297 fibroblasts, we failed to find a group equivalent to s-fibroblasts. Other cell populations seem to
298 be consistent to what has been found in other brain sites, like the intermediate
299 oligodendrocytes that are found enriched in the hypothalamus and the corpus callosum in
300 mice(*34*). In summary, these findings show that some cell populations may be specific to the
301 DVC compared to other brain sites and we were able to capture them in our atlas, further
302 supporting its utility for studying this brain region.
303
304 Within the mouse neural classes, we found overlap between *Cck* and *Th*-expressing cells. As
305 these cells have previously been described as non-overlapping, this was unexpected(*17*). Our
306 *in-situ* hybridization confirmed the presence of *Cck|Th* positive cells within the NTS and AP.
307 We believe the discrepancy may be due to detection methods as these cells were initially
308 defined as non-overlapping using immunofluorescent detection of *Th* protein and a *Cck*
309 genetic reporter(*17*). Within the NTS, *Cck* neurons are strongly aversive whereas *Th*-labelled
310 neurons are non-aversive(*50*). The role of dual Cck/Th positive neurons remains to be
311 determined. While no functional characterization of *Cck* and *Th* neurons of the AP has been
312 performed, we posit that as some *Th*-expressing AP neurons also express *Gfral* and *Casr*; both
313 having potently aversive ligands (e.g. GDF15, deoxynivalenol)(*16, 51*); they are likely to
314 mediate aversive anorexia.
315
316 Our snRNA-Seq data also resulted in detected transcripts for both *Agrp* and *Hcrt*. While both
317 neuropeptides have long been considered to have hypothalamic-exclusive expression, a
318 recent report describes *Agrp*-expressing cells within the mouse DVC(*46*). To confirm our
319 sequencing data, we performed *in-situ* hybridizations for both *Agrp* and *Hcrt* but failed to
320 detect any transcripts within the DVC, in agreement with this finding is that the mapped reads

321 within the *Agrp* and *Hcrt* gene overwhelmingly mapped to non-coding regions, suggesting to
322 us that the AGRP and HCRT neuropeptides are not produced by DVC cells in rodents.
323
324 Beside the classical dichotomy of inhibitory or GABAergic and excitatory glutamatergic,
325 neurons, subpopulations of neurons have been shown to be capable of co-releasing GABA
326 and glutamate(*52*) and other neurotransmitter combinations(*53*). By co-expression analysis of
327 genes implicated in synthesis or neurotransmitter vesicle packing, we confirmed that over 50%
328 the DVC neurons co-transmit/co-release more than one primary neurotransmitter. This complex
329 functionality of the DVC is further exemplified by the presence of neurons with seemingly mixed
330 programs which we called 'mixed neurons'. Similar groups have been described in the
331 hypothalamus(*37*) suggesting that some neurons may have hybrid-functionalities. As these
332 mixed neurons share transcriptomic features with many other cell identities, we foresee them
333 to be difficult to target or to be affected by treatments not directed to them as an off-target
334 effect. Finally, we were not able to clearly associate our neuronal classes with the cell classes
335 that had been previously identified in hypothalamic snRNA-seq data(*29*) which is in line with
336 the complementarity of different metabolic centers in the brain suggesting that the
337 hypothalamic and brain stem neuronal populations involved in feeding control and energy
338 balance, share only some functionality, possibly reflective of their complementary roles in
339 metabolic regulation.
340
341 To perform a cross-species analysis, we generated a rat-based DVC atlas and compared it
342 with the mouse DVC. Our rat dataset was smaller than the mouse data, it is possible some of
343 the of the new neuronal cell identities (e.g. M_sema, M4) may contain cells belonging to
344 multiple cell types, as treeArches did not appended these identities to the tree. Despite this,
345 we corroborated two new cell types in the rat DVC that are not present in mice the *Pdgfa*-
346 expressing (ortus-akin class) and the immunity-related neurons. *Pdgfra* is a well described
347 marker gene for OPCs and fibroblasts within the central nervous system(*45*) but, to our
348 knowledge, has not been associated with neurons. Notably, although the PDGFRA immuno-
349 signal in HuC/D+ neurons is clearly discernible, it is less intense than in OPCs and fibroblasts.
350 Since it was previously demonstrated that OPCs can give rise to neurons in the adult brain(*54*),
351 it is possible that these PDGFRA+/HuCD+ cells in the AP represent a transient stage of
352 PDGFRA+ OPCs differentiating into neurons.
353
354 Regardless of their maturity, we speculate that the Pdgfra neurons (ortus-akin class) have roles
355 in appetite regulation as they express leptin receptor and *Gfral*. Interestingly, while multiple
356 studies have failed to detect *Lepr* via Cre-based reporters(*38, 55*) or leptin-induced
357 phosphorylated STAT3 in the AP of mice(*56*), *Lepr* and leptin-induced phosphorylated STAT3

are detectable within the rat AP(*57-59*). We believe one explanation for this species discrepancy in *Lepr* expression is the absence of the ortus class neurons in mice.

DVC-targeting obesity therapeutics, including amylin and GLP1 mimetics, produce clinically relevant weight loss but are associated with multiple gastrointestinal adverse events and there is a need to develop new obesity therapies that can reduce appetite without unwanted gastrointestinal side effects(*60, 61*). Indeed, the DVC cells that regulate appetite suppression and nausea are separable(*50*), making targeting such cells an attractive target for pharmacotherapy. As meal consumption is generally not associated with gastrointestinal distress, we sought to identify refeeding responsive cells within the mouse DVC. From this analysis, we found nearly all neural cell identities are transcriptionally altered by meal consumption. Therefore, identifying neurons that promote non-aversive anorexia via the transcriptional response to refeeding as the basis of pharmacotherapy is unlikely to yield specific targetable pathways.

In general, the limitations of our study are that it is based on nuclear RNA which may reflect a fraction of biological changes, and that cell viability and isolating nuclei from cells are challenging. In addition, for meal consumption, we were unable to analyze responses in individual mice but due the number of cells recovered from each mouse DVC, pooling was the most amenable option in our pipeline.

As the amount of snRNA-Seq data performed on the DVC continues to grow, there is a need for a common, scalable label set that can be applied to new studies and integrate new sequencing data. To develop such a label set, we started with a *de novo* DVC atlas, we generated three layers of cellular granularity for both neural and non-neuronal cell types. Then, using the treeArches pipeline(*40*) we harmonized our snRNA-Seq labels with the Ludwig dataset(*2*) and increased our cellular granularity from three to four layers of resolution. This approach of manual curation and harmonization enhanced the reach of our cell atlas to capture the complexity of the DVC neurons since not all groups seem to contain easily delineable subgroups of cells. For example, eleven of the labels incorporated into our cell hierarchy in this pipeline belong to the monoaminergic neuronal class, which seem to encompass multiple subgroups of specialized cells. We further constructed the rodent DVC cell atlas which resulted in a fifth layer of cell identity to the monoaminergic M3 neurons. Although the number of identities increases as layers are more specific, this gives this unified atlas greater adaptability to different research needs. Additionally, our labels can be accurately harmonized with new databases regardless of size and new DVC snRNA-Seq data can be added to the tree to generate new branches. Thus, our unified rodent DVC atlas is highly amenable to future research elucidating new biologic and therapeutic insights into DVC cell types.

396

397 **Materials and methods**

398 Experimental design

399 To generate a snRNA-Seq based atlas of the mouse dorsal vagal complex (DVC), we isolated
400 the DVC from 30 adult C57BL/6J mice and subjected them to 10x Genomics-based single-
401 nuclei RNA barcoding and sequencing. Mice were either fasted overnight (n=5), fasted
402 overnight and then refed 2 hours prior to euthanasia (n=10), fed ad libitum (n=5), injected with
403 LiCl (n=5) or injected with vehicle (n=5). Conserved cell clusters across these groups were
404 then identified.

405

406 Animals

407 All animals were bred in the Unit for Laboratory Animal Medicine at the University of Michigan
408 and the Research Institute of the McGill University Health Centre. Procedures performed were
409 approved by the University of Michigan Committee on the Use and Care of Animals, in
410 accordance with Association for the Assessment and Approval of Laboratory Animal Care and
411 National Institutes of Health guidelines. Alternatively, procedures were approved by the animal
412 care committee of McGill University.

413

414 Mice for sn-RNA sequencing assay

415 Wild-type C57BL/6J mice (Jackson laboratories) were given ad libitum access to food (Purina
416 Lab Diet 5001) and water in temperature-controlled (22°C) rooms on a 12-hour light-dark cycle
417 with daily health checks. Mice were euthanized by isoflurane anesthesia and decapitated, then
418 the brain was removed from the skull and aligned in a brain matrix. The cerebellar cortex was
419 removed and the DVC was microdissected using AP-centric targeting and flash frozen in liquid
420 nitrogen. Frozen tissue was stored at -80°C until use.

421

422 For assessment of feeding-related gene expression, mice were either ad libitum fed or food
423 was removed at the onset of the dark cycle and the animals were fasted overnight. Animals
424 were then euthanized the next morning under ad libitum fed or fasting conditions. A subset of
425 fasted animals (n=5) were provided food and allowed to refeed for 2 hours prior to euthanasia.

426

427 Mice for *in-situ* hybridization assays

428 Mice were provided with ad libitum access to food (Purina Lab Diet 5001) and water in
429 temperature-controlled (22°C) rooms on a 12 h light-dark cycle with daily health status checks.
430 C57BL/6J mice (Jackson laboratories) were euthanized by isoflurane anesthesia followed by
431 CO_2 asphyxiation. Mice were then trans-cardially perfused with phosphate buffered saline for
432 3 minutes followed by 5 minutes perfusion with 10% formalin. Brain tissue was then collected

433 and postfixed for 24 hours in 10% formalin before transfer into 30% sucrose for a minimum of
434 24 hours. Brains were then sectioned as 30 μm thick, free floating sections.
435
436 Rats
437 Wild-type Sprague Dawley rats (Charles River) were provided with given access to food (Purina
438 Lab Diet 5001) and water in temperature-controlled (22°C) rooms on a 12-hour light-dark cycle
439 with daily health checks. Rats were euthanized by intraperitoneal injections of pentobarbital
440 and decapitated, then the brain was removed from the skull and aligned in a brain matrix. The
441 cerebellar cortex was removed and the DVC was dissected out in an AP-centric manner then
442 flash frozen in liquid nitrogen. Frozen tissue was stored at -80°C until use.
443
444 Isolation of nuclei from DVC tissue
445 Frozen tissue (from 2 to 3 mixed sex mice of the same treatment or 1 rat per sample) was
446 homogenized in Lysis Buffer (EZ Prep Nuclei Kit, Sigma-Aldrich) with Protector RNAase
447 Inhibitor (Sigma-Aldrich) and filtered through a 30mm MACS strainer (Miltenyi). Filtered
448 samples were centrifuged at 500 rcf for 5 minutes at 4°C, and pelleted nuclei were
449 resuspended in fresh-made wash buffer (10 mM Tris Buffer, pH 8.0, 5 mM KCl, 12.5 mM MgCl2,
450 1% BSA with RNAse inhibitor) before undergoing a second filtration and centrifugation. The
451 pelleted nuclei were resuspended in wash buffer with propidium iodide (Sigma-Aldrich) and
452 underwent FACS sorting on a MoFlo Astrios Cell Sorter to remove debris. PI+ nuclei were
453 collected and centrifuged at 100 rcf for 5 minutes at 4°C and resuspended in wash buffer to
454 obtain a concentration of 750-1,200 nuclei/μL in preparation for sequencing.
455
456 Single-nuclei RNA-sequencing
457 Library preparation was handled by the Advanced Genomics Core at the University of
458 Michigan. RT mix was added to target approximately 10,000 nuclei recovered per sample and
459 loaded onto the 10× Chromium Controller chip. The Chromium Single Cell 3′ Library and Gel
460 Bead Kit v3, Chromium Chip B Single Cell kit, and Chromium i7 Multiplex Kit were used for
461 subsequent RT, cDNA amplification, and library preparation, as instructed by the
462 manufacturer. Libraries were sequenced on an Illumina NovaSeq 6000 (pair ended with read
463 lengths of 150 nt).
464
465 Processing of the snRNA-seq files
466 From the snRNA-seq, we obtained four FASTQ files (two per sequencing lane, containing
467 forward and reverse sequences respectively) per mouse treatment and two files with the
468 forward and reverse sequences for the rat samples. We pre-processed the murine FASTQ files
469 using either CellRanger 5.0.1 with inclusion of introns or CellRanger 7.0.1 with default

470 parameters (which include intronic sequences) to align sequencing reads to the murine
471 genome(*21*). We aligned to the *Mus musculus* refdata-gex-mm10-2020-A reference genome.
472 For the rat files, we used CellRanger 3.0.1 with no introns inclusion and aligned using the *Rattus*
473 *norvegicus* genome assembly Rnor_6.0(*21*). We obtained 110,167 and 13,360 cells from the
474 murine and rat experiments, respectively. In addition to these two datasets, we also used the
475 following steps to process the murine Dowsett dataset(*18*) publicly available as a raw gene
476 expression matrix set of files. We processed the gene expression matrices in R(*62*) with Seurat
477 v5 and SeuratObject v5 to remove low quality cells(*63*). For processing and analysis, R
478 v.4.3.1(*62*) was used. We filtered cells with ≥500 number of genes mapped and >1.22 RNA
479 unique molecular identifiers (UMIs) counts/genes mapped ratio (based on the first 2
480 percentiles per sample) (**Table S10**). Subsequently, we merged the data per treatment,
481 calculated the median RNA content of clusters at resolution 1.0 and those below the first
482 quartile of the median distribution were removed (**Table S11**). Additionally, we used
483 DoubletFinder v.2.0.3 based on the expected doublets rates by 10X Genomics after adjusting
484 for homotypic doublets modeled as the sum of squared annotation frequencies(*64*) (**Table**
485 **S12**). On each iteration we processed the data with libraries scaled to 10,000 UMIs per cell
486 and log-normalized. We identified the most variable genes computing a bin Z-score for
487 dispersion based on 20 bins average expression. We regressed UMI counts and used
488 principal component (PC) analysis for dimensionality reduction on to the top 2,000 most
489 variable genes. We used the first 30 PCs for *k*-nearest neighbors clustering and for uniform
490 manifold approximation and projection (UMAP) projections using Seurat v5(*63*) default
491 parameters. Murine samples integration in a single matrix was done with Harmony(*65*), after
492 which clustering and UMAP projections were performed using the harmony embeddings
493 instead of PCs.
494
495 <u>Mapping of our murine data to existing brain databases</u>
496 We mapped the resulting murine integrated high quality singlets to the celldex v1.12.0 built-in
497 mouse RNA-seq reference and other four mouse databases(*37, 66-68*) (**Table S1**) using
498 SingleR v2.4.1(*69*) and scRNAseq v2.16.0(*70*) packages in R(*62*). Since each database has
499 its own cell type nomenclature, in our murine dataset we established a 'likely-cell type' to be
500 unanimous among all databases, for example if all databases labeled a cell as 'neuron'. We
501 initially labeled the cells with conflicting or unassigned label by one or more databases as
502 'unknown'. In order to confirm the cell type of all the cells labeled and to identify the unknown
503 cell identities, we mapped 473 markers from the literature. For this, the average expression per
504 marker gene was obtained on scaled data for each cluster at resolution 1.0 (i.e. 48 clusters)
505 (**Table S2**). We also manually visualized UMAP projections from all these markers in our
506 dataset. Some clusters (e.g. cluster 27) showed in the previous step to contain cells belonging
507 to different cell types, so we subset and reprocessed these clusters using the Harmony

508 embeddings to assign their cell identity based on marker expression at the smallest resolution
509 that allowed to separate them (Fig.S5).
510
511 Assigning high resolution clustering-based cell identity in the murine dataset
512 In the murine dataset, for all non-neuronal clusters at resolution 1.0 gene expression markers
513 were obtained using the FindConservedMarkers function from Seurat v5(*63*) package in R(*62*).
514 The function was run using the MAST algorithm(*71*) on scaled data with a log fold-change (FC)
515 threshold of 0.25. Only upregulated marker genes detected on 40% of all cells in that cluster,
516 were retained. Since the FindConservedMarkers gives a log2FC output per sample, we
517 calculated the average log2FC across samples and the proportion of samples for which a gene
518 had an adjusted p-value ≤0.05. A marker gene was considered as such if it had an average
519 log2FC>1 across samples and was significant (i.e. had an adjusted p-value ≤0.05) in more
520 than 80% of the samples. Furthermore, neurons were subset, reprocessed and subjected to
521 new clustering through Seurat v5(*63*). We obtained the gene markers per cluster at resolution
522 1.0 as described. We named the clusters based on the known functions of the
523 upregulated/downregulated genes (e.g. myelinating oligodendrocytes), peculiarities of the cell
524 groups (e.g. Ca^{+}-permeable astrocytes) or their upregulated gene expression markers if the
525 previous methods were unsuitable (e.g. Ano2 neurons) (Table S5). All visualizations, unless
526 otherwise stated, were done using ggplot2 v3.5.0 and ComplexHeatmap v2.18.0 packages in
527 R(*62*).
528
529 Oligodendrocytes trajectory inference
530 We subset the oligodendrocytes (i.e. pre-myelinating, myelinating intermediate and
531 myelinating) in our murine dataset and placed each cell on an inferred cellular trajectory using
532 their transcriptomic data in R(*62*). We used the SCORPIUS v1.0.9 package(*72*) with default
533 parameters to perform dimensionality reduction by PCA on log-normalized counts and to
534 obtain the trajectory image, with a random seed of 1,000. We additionally performed the
535 analysis on the Harmony embeddings from the original data integration.
536
537 Gene expression files format interconversions
538 To convert Seurat ('RDS') DVC datasets to 'h5ad' format and vice versa, we used reticulate
539 v1.35.0(*73*) and anndata 0.7.5.6(*74*) packages in R(*62*) with import of scipy, scanpy, numpy
540 and anndata modules from Python v3.9(*75*). To convert .csv and .tsv datasets (i.e. the Ludwig
541 dataset(*2*) and the cortex/hippocampus database(*33*)), we converted those to 'h5ad' format in
542 Python v3.9(*75*).
543

544 Murine DVC hierarchy construction
545 We converted our murine labeled count matrix to h5ad. We used treeArches(*40*) in Python
546 v3.9(*75*) to create a manual tree using the three layers of cellular granularity in our database.
547 We reprocessed the samples using the treeArches pipeline(*40*) to normalize the count data
548 (counts normalized per cell and then log-normalized), identify the top 2,500 most variable
549 genes and integrate the samples using scVI(*76*). This reference latent space obtained after
550 integration was used to generate the UMAP embeddings. We trained our manual tree based
551 on the cell identity layer-3 labels using default parameters.
552
553 We subset the Ludwig dataset to match the initial 2,500 most variable genes from our datasets
554 and performed surgery to incorporate labels from the Ludwig dataset(*2*). The two layers of
555 granularity established by Ludwig(*2*) were combined in the variable "identity_layer3" to contain
556 the highest granularity of cell identity for neurons and non-neuronal cell types. Next, we
557 normalized the count data as specified for our murine dataset, and mapped the Ludwig dataset
558 on the reference latent space using scArches. We then used the learn_tree function with default
559 parameters for hierarchical progressive learning from scHPL v1.0.5(*41*) which yielded a
560 hierarchy of harmonized cell labels from both datasets. We printed all trees using matplotlib
561 v3.8.2(*77*) and scHPL v1.0.5(*41*). All steps performed and scripts used in this phase are
562 available in the GitHub repository: https://github.com/LabSabatini/DVC_cell_atlas.
563
564 Corroboration of the validity of our murine cell hierarchy using treeArches prediction modality
565 Using treeArches(*40*) and its dependencies in Python v3.9(*75*) we compared the original cell
566 labels in our and Ludwig datasets with the resulting prediction of the label for each cell using
567 our learned hierarchy. We used the predict_labels function from scHPL v1.0.5(*41*) with default
568 parameters, and the latent representation obtained when we constructed our murine hierarchy.
569 We compared the original and the predicted labels through a heatmap visualization. Next, we
570 predicted the labels of new data, a murine dataset by Dowsett which comprises the NTS, a
571 part of the DVC(*18*). We processed the Dowsett data similarly to the Ludwig dataset and
572 obtained the query latent representation. We then used the predict_labels function from scHPL
573 v1.0.5(*41*) with default parameters to transfer the labels in our hierarchy to the Dowsett dataset
574 based on gene expression similarity among the 2,500 initial most variable genes. We then
575 compared the resulting labels from this prediction to the manual mapping of our cell identities
576 based on maker expression (**Table S3**) using UMAP embeddings in R(*62*).
577
578 Labeling of our rat DVC dataset
579 We processed our rat dataset as previously described to obtain high-quality singlets. Based
580 on the three layers of cell identity that we created to label the murine data from our experiments,
581 we calculated the average expression of the top 5 marker genes for each of the layer-3

identities (except duplicated genes and mouse-specific genes) on every rat cluster to identify those that were equivalent and could be labeled as the murine data (**Tables S5** and **S6**). Since this dataset is smaller than the mouse data, we decided to use clusters at resolution of 2.0 to capture more heterogeneity and delineate better the non-neuronal cell populations. Clusters 27 and 29 were further subset and reclustered since we found them to contain a mix of endothelial cells, mural cells, tanycytes and fibroblasts based on marker expression. The smallest resolution that allowed to separate these populations was used to label the cells. Neurons were also subset and we mapped the murine neuronal classes markers to resolution 2.0 markers which were manually curated to delineate better the different populations within them. For all cell identities, and because we only applied one treatment to the rats (i.e. fed ad libitum), we used the FindMarkers function from Seurat v5(*63*) package in R(*62*) to obtain gene expression markers of each rat cell population. The function was run using the MAST algorithm(*71*) with same parameters used for the murine data (**Table S7**).

Construction of the rodent DVC hierarchy

We then integrated our rat labeled dataset to the murine samples in Python v3.9(*75*) using the initial top 2,500 most variable genes initially defined in our mouse data. Incorporation of rat labels was done as previously described for the Ludwig dataset using the learn_tree function for hierarchical progressive learning from scHPL v1.0.5(*41*). The cell populations that were not rejected but placed at the bottom of the tree were moved manually to their belonging parent branches (**Fig.8A**; **Fig.S10**). For example, the 'smooth_muscle_rat' label was moved to be a children node of the mural cells node (**Fig.8A**). If the parent branch did not exist, we created it. For example, the 'immunity_related_rat' label belonged to a new rat neuronal class, therefore, we incorporated this parent node within the neurons node and then we moved the 'immunity_related_rat' label to be a children node (**Fig.8A**). After manual curation, we re-trained the tree. We printed all trees using matplotlib v3.8.2(*77*) and scHPL v1.0.5(*41*). All steps performed and scripts used in this phase are available at the GitHub repository https://github.com/LabSabatini/DVC_cell_atlas for reproducibility.

Mapping gene expression in other brain-site snRNA-seq datasets

We downloaded labeled datasets from two brain regions different from the DVC: the HypoMap(*29*) and the cortex/hippocampus databases(*33*). For the HypoMap data, we subset the database by randomly selecting cells belonging to 32 included hypothalamic samples. We processed the datasets in Seurat v5(*63*) as previously described and obtained Harmony(*65*) embeddings to obtain UMAP projections. The labels used in the visualization are the original curated labels provided on each dataset. Neurons were further subset from the processed datasets and reprocessed as previously described. The cortex/hippocampus dataset was

619 processed in the same manner, except that since it mainly contained astrocytes, these were
620 subset.
621
622 Differential gene expression analysis in murine treatments
623 We subset the murine dataset neurons and glial cells at layer 2 granularity of identity and
624 obtained differential gene expression for pair-wise comparison of treatments (i.e. refed versus
625 ad libitum fed, refed versus fasted and LiCl versus vehicle injected mice). We used the
626 FindMarkers function from Seurat v5(*63*) package in R(*62*) using the MAST algorithm(*71*) on
627 log-normalized counts with a minimal log fold-change threshold of 0.1 and default parameters.
628 The number of cells per treatment can be found in **Table S13**.
629
630 Immunofluorescent staining
631 Free-floating brain sections from mouse and rat were washed with PBS, three times for five
632 minutes. The sections were then blocked for one hour in PBS containing 0.1% Triton X-100 and
633 3% normal donkey serum (Fisher Scientific). The sections were incubated overnight at room
634 temperature with Goat anti-PDGFRA (Invitrogen, CAT#, 1:200), HuC/HuD (Invitrogen, A-21271,
635 1:30). The following day, sections were washed and incubated for two hours with Alexflour488
636 and Cy3 conjugated secondary antibody (Jackson immunoresearch, 1:500). Tissues were then
637 washed three times in PBS before being mounted onto glass slides, covered in mounting media
638 (Fluoromount-G, Southern Biotechnology) and coverslipped. Imaging was performed using an
639 Olympus BX61 microscope and a Zeiss LSM780-NLO laser scanning confocal microscope
640 equipped with IR-OPO lasers at the Molecular Imaging Platform, Research Institute of the
641 McGill University Health Centre (RI-MUHC), Montreal, CA.
642
643 *In-situ* hybridization and imaging
644 Brain sections containing the DVC from four wild-type C57BL/6J mice obtained as previously
645 described, were fixed on glass slides and stored at -20°C for no more than 36 hours. We
646 followed the manufacturer's ACD 323100 user manual for the RNAscope® Multiplex
647 Fluorescent Reagent Kit v2 Assay for fixed frozen tissue samples. Briefly, we rinsed the slides
648 with 1X PBS and incubated them at room temperature (RT) for 10 minutes after adding ~1-2
649 drops of H_2O_2 per section. We removed the H_2O_2 from slides and rinsed them twice with distilled
650 water (diH_2O). Next, we submerged the slides in 200 mL of hot diH_2O for 10 seconds followed
651 by 200mL of RNAscope® 1X Target Retrieval Reagent for 5 minutes, using a steamer with lid.
652 After briefly transferring the slides to RT diH_2O, we submerged them in 100% ethanol for 3
653 minutes and allowed them to air dry. We applied approximately 1-2 drops of RNAscope®
654 Protease III to each section and incubated them at 40°C for 30 minutes in a HybEZ™ oven with

655 diH_2O wet paper in the tray. After rinsing the slides with diH_2O, we hybridized the probes at
656 40°C for 2 hours.
657
658 From this point on, we performed all steps by incubating the slides at 40°C in the HybEZ™
659 oven with humid tray followed by rinse using RNAscope® 1X Wash Buffer. We applied
660 approximately 1-2 drops of RNAscope® reagents AMP1, AMP2, AMP3 and then intercalated
661 HRP channel (15 minutes), fluorophore (30 minutes) and HRP blocker (15 minutes) for each
662 channel present in the probe mix. The mix of probes used for the *Th*|*Cck* co-expression assay
663 was RNAscope® Mm-Th-C2 (317621-C2) and Mm-Cck-C3 (402271-C3) diluted in probe
664 diluent as specified in the user manual. For *Hcrt* we used RNAscope® Mm-Hcrt-C2 (490461-
665 C2) and for *Agrp*, Mm-Agrp (400711), in a dilution as specified in the user manual. The used
666 fluorophores were Cy3 for *Cck* and *Hcrt* (1:1,500), and Cy5 for *Th* and *Agrp* (1:1,000) diluted
667 in RNAscope® TSA buffer. DAPI dye (1:1,000) was applied at the end of the assay, and the
668 samples were stored for ~48 hours at -4°C, protected from light, before imaging. We imaged
669 the sections using a Zeiss LSM780-NLO laser scanning confocal microscope with IR-OPO
670 lasers at the Molecular Imaging Platform at the RI-MUHC, Montreal, CA.
671

672 **References**

673 1. L. Gautron, J. K. Elmquist, K. W. Williams, Neural control of energy balance: translating
674 circuits to therapies. *Cell* **161**, 133-145 (2015).
675 2. M. Q. Ludwig, W. Cheng, D. Gordian, J. Lee, S. J. Paulsen, S. N. Hansen, K. L.
676 Egerod, P. Barkholt, C. J. Rhodes, A. Secher, L. B. Knudsen, C. Pyke, M. G. Myers,
677 Jr., T. H. Pers, A genetic map of the mouse dorsal vagal complex and its role in
678 obesity. *Nat Metab* **3**, 530-545 (2021).
679 3. L. Bai, S. Mesgarzadeh, K. S. Ramesh, E. L. Huey, Y. Liu, L. A. Gray, T. J. Aitken, Y.
680 Chen, L. R. Beutler, J. S. Ahn, L. Madisen, H. Zeng, M. A. Krasnow, Z. A. Knight,
681 Genetic Identification of Vagal Sensory Neurons That Control Feeding. *Cell* **179**, 1129-
682 1143 e1123 (2019).
683 4. W. Han, L. A. Tellez, M. H. Perkins, I. O. Perez, T. Qu, J. Ferreira, T. L. Ferreira, D.
684 Quinn, Z. W. Liu, X. B. Gao, M. M. Kaelberer, D. V. Bohorquez, S. J. Shammah-
685 Lagnado, G. de Lartigue, I. E. de Araujo, A Neural Circuit for Gut-Induced Reward.
686 *Cell* **175**, 665-678 e623 (2018).
687 5. E. K. Williams, R. B. Chang, D. E. Strochlic, B. D. Umans, B. B. Lowell, S. D. Liberles,
688 Sensory Neurons that Detect Stretch and Nutrients in the Digestive System. *Cell* **166**,
689 209-221 (2016).
690 6. M. W. Schwartz, Central nervous system regulation of food intake. *Obesity (Silver*
691 *Spring)* **14 Suppl 1**, 1S-8S (2006).
692 7. W. Cheng, E. Ndoka, J. N. Maung, W. Pan, A. C. Rupp, C. J. Rhodes, D. P. Olson, M.
693 G. Myers, Jr., NTS Prlh overcomes orexigenic stimuli and ameliorates dietary and
694 genetic forms of obesity. *Nat Commun* **12**, 5175 (2021).
695 8. W. Qiu, C. R. Hutch, Y. Wang, J. Wloszek, R. A. Rucker, M. G. Myers, D. Sandoval,
696 Multiple NTS neuron populations cumulatively suppress food intake. *Elife* **12**, (2023).
697 9. T. Borner, C. G. Liberini, T. A. Lutz, T. Riediger, Brainstem GLP-1 signalling
698 contributes to cancer anorexia-cachexia syndrome in the rat. *Neuropharmacology*
699 **131**, 282-290 (2018).

10. C. W. le Roux, O. Steen, K. J. Lucas, E. Startseva, A. Unseld, A. M. Hennige, Glucagon and GLP-1 receptor dual agonist survodutide for obesity: a randomised, double-blind, placebo-controlled, dose-finding phase 2 trial. *Lancet Diabetes Endocrinol* **12**, 162-173 (2024).
11. S. M. Advani, P. G. Advani, H. M. VonVille, S. H. Jafri, Pharmacological management of cachexia in adult cancer patients: a systematic review of clinical trials. *BMC Cancer* **18**, 1174 (2018).
12. M. M. Veniant, S. C. Lu, L. Atangan, R. Komorowski, S. Stanislaus, Y. Cheng, B. Wu, J. R. Falsey, T. Hager, V. A. Thomas, M. Ambhaikar, L. Sharpsten, Y. Zhu, V. Kurra, R. Jeswani, R. K. Oberoi, J. R. Parnes, N. Honarpour, J. Neutel, J. L. Strande, A GIPR antagonist conjugated to GLP-1 analogues promotes weight loss with improved metabolic parameters in preclinical and phase 1 settings. *Nat Metab* **6**, 290-303 (2024).
13. J. M. Adams, H. Pei, D. A. Sandoval, R. J. Seeley, R. B. Chang, S. D. Liberles, D. P. Olson, Liraglutide Modulates Appetite and Body Weight Through Glucagon-Like Peptide 1 Receptor-Expressing Glutamatergic Neurons. *Diabetes* **67**, 1538-1548 (2018).
14. K. P. Huang, A. A. Acosta, M. Y. Ghidewon, A. D. McKnight, M. S. Almeida, N. T. Nyema, N. D. Hanchak, N. Patel, Y. S. K. Gbenou, A. E. Adriaenssens, K. A. Bolding, A. L. Alhadeff, Dissociable hindbrain GLP1R circuits for satiety and aversion. *Nature* **632**, 585-593 (2024).
15. I. Medic, S. Gulati, H.-J. Lenz, D. Mahalingam, J. Thomas, J. Luo, J. Zha, A. DePaoli, C. Tran-Muchowski, C. Tseng, H. Lieu, Initial results of a cohort of advanced prostate cancer patients in a phase Ia study of NGM120, a first-in-class anti- GDNF family receptor alpha like (GFRAL) antibody. *Annals of Oncology* **33**, S1186-S1186 (2022).
16. L. Yang, C. C. Chang, Z. Sun, D. Madsen, H. Zhu, S. B. Padkjaer, X. Wu, T. Huang, K. Hultman, S. J. Paulsen, J. Wang, A. Bugge, J. B. Frantzen, P. Norgaard, J. F. Jeppesen, Z. Yang, A. Secher, H. Chen, X. Li, L. M. John, B. Shan, Z. He, X. Gao, J. Su, K. T. Hansen, W. Yang, S. B. Jorgensen, GFRAL is the receptor for GDF15 and is required for the anti-obesity effects of the ligand. *Nat Med* **23**, 1158-1166 (2017).
17. C. W. Roman, S. R. Sloat, R. D. Palmiter, A tale of two circuits: CCK(NTS) neuron stimulation controls appetite and induces opposing motivational states by projections to distinct brain regions. *Neuroscience* **358**, 316-324 (2017).
18. G. K. C. Dowsett, B. Y. H. Lam, J. A. Tadross, I. Cimino, D. Rimmington, A. P. Coll, J. Polex-Wolf, L. B. Knudsen, C. Pyke, G. S. H. Yeo, A survey of the mouse hindbrain in the fed and fasted states using single-nucleus RNA sequencing. *Mol Metab* **53**, 101240 (2021).
19. C. Zhang, J. A. Kaye, Z. Cai, Y. Wang, S. L. Prescott, S. D. Liberles, Area Postrema Cell Types that Mediate Nausea-Associated Behaviors. *Neuron* **109**, 461-472 e465 (2021).
20. S. M. Fortin, R. K. Lipsky, R. Lhamo, J. Chen, E. Kim, T. Borner, H. D. Schmidt, M. R. Hayes, GABA neurons in the nucleus tractus solitarius express GLP-1 receptors and mediate anorectic effects of liraglutide in rats. *Sci Transl Med* **12**, (2020).
21. G. X. Zheng, J. M. Terry, P. Belgrader, P. Ryvkin, Z. W. Bent, R. Wilson, S. B. Ziraldo, T. D. Wheeler, G. P. McDermott, J. Zhu, M. T. Gregory, J. Shuga, L. Montesclaros, J. G. Underwood, D. A. Masquelier, S. Y. Nishimura, M. Schnall-Levin, P. W. Wyatt, C. M. Hindson, R. Bharadwaj, A. Wong, K. D. Ness, L. W. Beppu, H. J. Deeg, C. McFarland, K. R. Loeb, W. J. Valente, N. G. Ericson, E. A. Stevens, J. P. Radich, T. S. Mikkelsen, B. J. Hindson, J. H. Bielas, Massively parallel digital transcriptional profiling of single cells. *Nat Commun* **8**, 14049 (2017).
22. C. E. Vaaga, M. Borisovska, G. L. Westbrook, Dual-transmitter neurons: functional implications of co-release and co-transmission. *Curr Opin Neurobiol* **29**, 25-32 (2014).
23. N. X. Tritsch, A. J. Granger, B. L. Sabatini, Mechanisms and functions of GABA co-release. *Nat Rev Neurosci* **17**, 139-145 (2016).
24. C. F. Landry, J. A. Ellison, T. M. Pribyl, C. Campagnoni, K. Kampf, A. T. Campagnoni, Myelin basic protein gene expression in neurons: developmental and regional

756 changes in protein targeting within neuronal nuclei, cell bodies, and processes. *J.*
757 *Neurosci.* **16**, 2452-2462 (1996).
758 25. D. Lutz, G. Loers, R. Kleene, I. Oezen, H. Kataria, N. Katagihallimath, I. Braren, G.
759 Harauz, M. Schachner, Myelin basic protein cleaves cell adhesion molecule L1 and
760 promotes neuritogenesis and cell survival. *J Biol Chem* **289**, 13503-13518 (2014).
761 26. V. T. Cheli, D. A. Santiago Gonzalez, V. Spreuer, V. Handley, A. T. Campagnoni, P. M.
762 Paez, Golli Myelin Basic Proteins Modulate Voltage-Operated Ca(++) Influx and
763 Development in Cortical and Hippocampal Neurons. *Mol Neurobiol* **53**, 5749-5771
764 (2016).
765 27. M. Melone, S. Ciappelloni, F. Conti, Plasma membrane transporters GAT-1 and GAT-3
766 contribute to heterogeneity of GABAergic synapses in neocortex. *Front Neuroanat* **8**,
767 72 (2014).
768 28. S. M. Theparambil, P. S. Hosford, I. Ruminot, O. Kopach, J. R. Reynolds, P. Y.
769 Sandoval, D. A. Rusakov, L. F. Barros, A. V. Gourine, Astrocytes regulate brain
770 extracellular pH via a neuronal activity-dependent bicarbonate shuttle. *Nat Commun*
771 **11**, 5073 (2020).
772 29. L. Steuernagel, B. Y. H. Lam, P. Klemm, G. K. C. Dowsett, C. A. Bauder, J. A. Tadross,
773 T. S. Hitschfeld, A. Del Rio Martin, W. Chen, A. J. de Solis, H. Fenselau, P. Davidsen, I.
774 Cimino, S. N. Kohnke, D. Rimmington, A. P. Coll, A. Beyer, G. S. H. Yeo, J. C. Bruning,
775 HypoMap-a unified single-cell gene expression atlas of the murine hypothalamus. *Nat*
776 *Metab* **4**, 1402-1419 (2022).
777 30. Y. Kubo, T. J. Baldwin, Y. N. Jan, L. Y. Jan, Primary structure and functional
778 expression of a mouse inward rectifier potassium channel. *Nature* **362**, 127–133
779 (1993).
780 31. N. Burnashev, A. Khodorova, P. Jonas, P. J. Helm, W. Wisden, H. Monyer, P. H.
781 Seeburg, B. Sakmann, Calcium-Permeable AMPA-Kainate Receptors in Fusiform
782 Cerebellar Glial Cells. *Science* **256**, 1566-1570 (1992).
783 32. J. R. P. Geiger, T. Melcher, D. S. Koh, B. Sakmann, S. P. H., P. Jonas, H. Monyer,
784 Relative Abundance of Subunit mRNAs Determines Gating and Ca*+ Permeability of
785 AMPA Receptors in Principal Neurons and Interneurons in Rat CNS. *Neuron* **15**, 193-
786 204 (1995).
787 33. M. Y. Batiuk, A. Martirosyan, J. Wahis, F. de Vin, C. Marneffe, C. Kusserow, J.
788 Koeppen, J. F. Viana, J. F. Oliveira, T. Voet, C. P. Ponting, T. G. Belgard, M. G. Holt,
789 Identification of region-specific astrocyte subtypes at single cell resolution. *Nat*
790 *Commun* **11**, 1220 (2020).
791 34. S. Marques, A. Zeisel, S. Codeluppi, D. van Bruggen, A. Mendanha Falcao, L. Xiao, H.
792 Li, M. Haring, H. Hochgerner, R. A. Romanov, D. Gyllborg, A. Munoz Manchado, G. La
793 Manno, P. Lonnerberg, E. M. Floriddia, F. Rezayee, P. Ernfors, E. Arenas, J. Hjerling-
794 Leffler, T. Harkany, W. D. Richardson, S. Linnarsson, G. Castelo-Branco,
795 Oligodendrocyte heterogeneity in the mouse juvenile and adult central nervous
796 system. *Science* **352**, 1326-1329 (2016).
797 35. M. Kasai, Y. Omae, Y. Kawai, A. Shibata, A. Hoshino, M. Mizuguchi, K. Tokunaga,
798 GWAS identifies candidate susceptibility loci and microRNA biomarkers for acute
799 encephalopathy with biphasic seizures and late reduced diffusion. *Sci Rep* **12**, 1332
800 (2022).
801 36. A. B. DePaula-Silva, C. Gorbea, D. J. Doty, J. E. Libbey, J. M. S. Sanchez, T. J. Hanak,
802 D. Cazalla, R. S. Fujinami, Differential transcriptional profiles identify microglial- and
803 macrophage-specific gene markers expressed during virus-induced
804 neuroinflammation. *J Neuroinflammation* **16**, 152 (2019).
805 37. J. N. Campbell, E. Z. Macosko, H. Fenselau, T. H. Pers, A. Lyubetskaya, D. Tenen, M.
806 Goldman, A. M. Verstegen, J. M. Resch, S. A. McCarroll, E. D. Rosen, B. B. Lowell, L.
807 T. Tsai, A molecular census of arcuate hypothalamus and median eminence cell
808 types. *Nat Neurosci* **20**, 484-496 (2017).
809 38. W. Cheng, E. Ndoka, C. Hutch, K. Roelofs, A. MacKinnon, B. Khoury, J. Magrisso, K.
810 S. Kim, C. J. Rhodes, D. P. Olson, R. J. Seeley, D. Sandoval, M. G. Myers, Jr., Leptin
811 receptor-expressing nucleus tractus solitarius neurons suppress food intake
812 independently of GLP1 in mice. *JCI Insight* **5**, (2020).

39. A. A. Worth, R. Shoop, K. Tye, C. H. Feetham, G. D'Agostino, G. T. Dodd, F. Reimann, F. M. Gribble, E. C. Beebe, J. D. Dunbar, J. T. Alexander-Chacko, D. K. Sindelar, T. Coskun, P. J. Emmerson, S. M. Luckman, The cytokine GDF15 signals through a population of brainstem cholecystokinin neurons to mediate anorectic signalling. *Elife* **9**, (2020).
40. L. Michielsen, M. Lotfollahi, D. Strobl, L. Sikkema, M. J. T. Reinders, F. J. Theis, A. Mahfouz, Single-cell reference mapping to construct and extend cell-type hierarchies. *NAR Genom Bioinform* **5**, lqad070 (2023).
41. L. Michielsen, M. J. T. Reinders, A. Mahfouz, Hierarchical progressive learning of cell identities in single-cell data. *Nat Commun* **12**, 2799 (2021).
42. V. Chou, R. V. Pearse, 2nd, A. J. Aylward, N. Ashour, M. Taga, G. Terzioglu, M. Fujita, S. B. Fancher, A. Sigalov, C. R. Benoit, H. Lee, M. Lam, N. T. Seyfried, D. A. Bennett, P. L. De Jager, V. Menon, T. L. Young-Pearse, INPP5D regulates inflammasome activation in human microglia. *Nat Commun* **14**, 7552 (2023).
43. S. O. Kleeman, T. M. Thakir, B. Demestichas, N. Mourikis, D. Loiero, M. Ferrer, S. Bankier, Y. Riazat-Kesh, H. Lee, D. Chantzichristos, C. Regan, J. Preall, S. Sinha, N. Rosin, B. Yipp, L. G. N. de Almeida, J. Biernaskie, A. Dufour, P. Tober-Lau, A. Ruusalepp, J. L. M. Bjorkegren, M. Ralser, F. Kurth, V. Demichev, T. Heywood, Q. Gao, G. Johannsson, V. H. Koelzer, B. R. Walker, H. V. Meyer, T. Janowitz, Cystatin C is glucocorticoid responsive, directs recruitment of Trem2+ macrophages, and predicts failure of cancer immunotherapy. *Cell Genom* **3**, 100347 (2023).
44. N. Hagan, J. L. Kane, D. Grover, L. Woodworth, C. Madore, J. Saleh, J. Sancho, J. Liu, Y. Li, J. Proto, M. Zelic, A. Mahan, M. Kothe, A. A. Scholte, M. Fitzgerald, B. Gisevius, A. Haghikia, O. Butovsky, D. Ofengeim, CSF1R signaling is a regulator of pathogenesis in progressive MS. *Cell Death Dis* **11**, 904 (2020).
45. S. H. Kang, M. Fukaya, J. K. Yang, J. D. Rothstein, D. E. Bergles, NG2+ CNS glial progenitors remain committed to the oligodendrocyte lineage in postnatal life and following neurodegeneration. *Neuron* **68**, 668-681 (2010).
46. T. P. Bachor, E. Hwang, E. Yulyaningsih, K. Attal, F. Mifsud, V. Pham, E. Vagena, R. Huarcaya, M. Valdearcos, C. Vaisse, K. W. Williams, P. J. Emmerson, A. W. Xu, Identification of AgRP cells in the murine hindbrain that drive feeding. *Mol Metab* **80**, 101886 (2024).
47. M. K. Holt, The ins and outs of the caudal nucleus of the solitary tract: An overview of cellular populations and anatomical connections. *J Neuroendocrinol* **34**, e13132 (2022).
48. D. M. Breen, H. Kim, D. Bennett, R. A. Calle, S. Collins, R. M. Esquejo, T. He, S. Joaquim, A. Joyce, M. Lambert, L. Lin, B. Pettersen, S. Qiao, M. Rossulek, G. Weber, Z. Wu, B. B. Zhang, M. J. Birnbaum, GDF-15 Neutralization Alleviates Platinum-Based Chemotherapy-Induced Emesis, Anorexia, and Weight Loss in Mice and Nonhuman Primates. *Cell Metab* **32**, 938-950 e936 (2020).
49. K. Tsuzuki, S. Ishiuchi, GluR2 expressed by glial fibrillary acidic protein promoter decreases the number of neurons. *Front. Biosci. (Landmark Ed)* **13**, 2784–2796 (2008).
50. W. Cheng, I. Gonzalez, W. Pan, A. H. Tsang, J. Adams, E. Ndoka, D. Gordian, B. Khoury, K. Roelofs, S. S. Evers, A. MacKinnon, S. Wu, H. Frikke-Schmidt, J. N. Flak, J. L. Trevaskis, C. J. Rhodes, S. I. Fukada, R. J. Seeley, D. A. Sandoval, D. P. Olson, C. Blouet, M. G. Myers, Jr., Calcitonin Receptor Neurons in the Mouse Nucleus Tractus Solitarius Control Energy Balance via the Non-aversive Suppression of Feeding. *Cell Metab* **31**, 301-312 e305 (2020).
51. A. R. Patel, H. Frikke-Schmidt, P. V. Sabatini, A. C. Rupp, D. A. Sandoval, M. G. Myers, Jr., R. J. Seeley, Neither GLP-1 receptors nor GFRAL neurons are required for aversive or anorectic response to DON (vomitoxin). *Am J Physiol Regul Integr Comp Physiol* **324**, R635-644 (2023).
52. D. H. Root, C. A. Mejias-Aponte, S. Zhang, H. L. Wang, A. F. Hoffman, C. R. Lupica, M. Morales, Single rodent mesohabenular axons release glutamate and GABA. *Nat Neurosci* **17**, 1543-1551 (2014).

53. A. Saunders, A. J. Granger, B. L. Sabatini, Corelease of acetylcholine and GABA from cholinergic forebrain neurons. *Elife* **4**, (2015).
54. S. C. Robins, E. Trudel, O. Rotondi, X. Liu, T. Djogo, D. Kryzskaya, C. W. Bourque, M. V. Kokoeva, Evidence for NG2-glia derived, adult-born functional neurons in the hypothalamus. *PLoS One* **8**, e78236 (2013).
55. N. Wada, S. Hirako, F. Takenoya, H. Kageyama, M. Okabe, S. Shioda, Leptin and its receptors. *J Chem Neuroanat* **61-62**, 191-199 (2014).
56. H. Munzberg, J. S. Flier, C. Bjorbaek, Region-specific leptin resistance within the hypothalamus of diet-induced obese mice. *Endocrinology* **145**, 4880-4889 (2004).
57. P. M. Smith, P. Brzezinska, F. Hubert, A. Mimee, D. H. Maurice, A. V. Ferguson, Leptin influences the excitability of area postrema neurons. *Am J Physiol Regul Integr Comp Physiol* **310**, R440-448 (2016).
58. C. G. Liberini, C. N. Boyle, C. Cifani, M. Venniro, B. T. Hope, T. A. Lutz, Amylin receptor components and the leptin receptor are co-expressed in single rat area postrema neurons. *Eur J Neurosci* **43**, 653-661 (2016).
59. L. Huo, L. Maeng, C. Bjorbaek, H. J. Grill, Leptin and the control of food intake: neurons in the nucleus of the solitary tract are activated by both gastric distension and leptin. *Endocrinology* **148**, 2189-2197 (2007).
60. S. R. Smith, L. J. Aronne, C. M. Burns, N. C. Kesty, A. E. Halseth, C. Weyer, Sustained weight loss following 12-month pramlintide treatment as an adjunct to lifestyle intervention in obesity. *Diabetes Care* **31**, 1816-1823 (2008).
61. J. P. H. Wilding, R. L. Batterham, S. Calanna, M. Davies, L. F. Van Gaal, I. Lingvay, B. M. McGowan, J. Rosenstock, M. T. D. Tran, T. A. Wadden, S. Wharton, K. Yokote, N. Zeuthen, R. F. Kushner, S. S. Group, Once-Weekly Semaglutide in Adults with Overweight or Obesity. *N Engl J Med* **384**, 989-1002 (2021).
62. R. C. Team. (R Foundation for Statistical Computing, Vienna, Austria, 2023).
63. Y. Hao, T. Stuart, M. H. Kowalski, S. Choudhary, P. Hoffman, A. Hartman, A. Srivastava, G. Molla, S. Madad, C. Fernandez-Granda, R. Satija, Dictionary learning for integrative, multimodal and scalable single-cell analysis. *Nat Biotechnol* **42**, 293-304 (2024).
64. C. S. McGinnis, L. M. Murrow, Z. J. Gartner, DoubletFinder: Doublet Detection in Single-Cell RNA Sequencing Data Using Artificial Nearest Neighbors. *Cell Syst* **8**, 329-337 e324 (2019).
65. I. Korsunsky, N. Millard, J. Fan, K. Slowikowski, F. Zhang, K. Wei, Y. Baglaenko, M. Brenner, P. R. Loh, S. Raychaudhuri, Fast, sensitive and accurate integration of single-cell data with Harmony. *Nat Methods* **16**, 1289-1296 (2019).
66. R. Chen, X. Wu, L. Jiang, Y. Zhang, Single-Cell RNA-Seq Reveals Hypothalamic Cell Diversity. *Cell Rep* **18**, 3227-3241 (2017).
67. R. A. Romanov, A. Zeisel, J. Bakker, F. Girach, A. Hellysaz, R. Tomer, A. Alpar, J. Mulder, F. Clotman, E. Keimpema, B. Hsueh, A. K. Crow, H. Martens, C. Schwindling, D. Calvigioni, J. S. Bains, Z. Mate, G. Szabo, Y. Yanagawa, M. D. Zhang, A. Rendeiro, M. Farlik, M. Uhlen, P. Wulff, C. Bock, C. Broberger, K. Deisseroth, T. Hokfelt, S. Linnarsson, T. L. Horvath, T. Harkany, Molecular interrogation of hypothalamic organization reveals distinct dopamine neuronal subtypes. *Nat Neurosci* **20**, 176-188 (2017).
68. B. Tasic, V. Menon, T. N. Nguyen, T. K. Kim, T. Jarsky, Z. Yao, B. Levi, L. T. Gray, S. A. Sorensen, T. Dolbeare, D. Bertagnolli, J. Goldy, N. Shapovalova, S. Parry, C. Lee, K. Smith, A. Bernard, L. Madisen, S. M. Sunkin, M. Hawrylycz, C. Koch, H. Zeng, Adult mouse cortical cell taxonomy revealed by single cell transcriptomics. *Nat Neurosci* **19**, 335-346 (2016).
69. D. Aran, A. P. Looney, L. Liu, E. Wu, V. Fong, A. Hsu, S. Chak, R. P. Naikawadi, P. J. Wolters, A. R. Abate, A. J. Butte, M. Bhattacharya, Reference-based analysis of lung single-cell sequencing reveals a transitional profibrotic macrophage. *Nat Immunol* **20**, 163-172 (2019).
70. D. Risso, M. Cole. (2023).
71. G. Finak, A. McDavid, M. Yajima, J. Deng, V. Gersuk, A. K. Shalek, C. K. Slichter, H. W. Miller, M. J. McElrath, M. Prlic, P. S. Linsley, R. Gottardo, MAST: a flexible statistical

926 framework for assessing transcriptional changes and characterizing heterogeneity in
927 single-cell RNA sequencing data. *Genome Biol* **16**, 278 (2015).
928 72. R. Cannoodt, W. Saelens, D. Sichien, S. Tavernier, S. Janssens, M. Guilliams, B.
929 Lambrecht, K. De Preter, Y. Saeys, SCORPIUS improves trajectory inference and
930 identifies novel modules in dendritic cell development. *Preprint at bioRxiv*, (2016).
931 73. K. Ushey, J. Allaire, Y. Tang. (2024).
932 74. R. Cannoodt. (2023).
933 75. G. Van Rossum, F. L. Drake. (CreateSpace, Scotts Valley, CA, 2009).
934 76. A. Gayoso, R. Lopez, G. Xing, P. Boyeau, V. Valiollah Pour Amiri, J. Hong, K. Wu, M.
935 Jayasuriya, E. Mehlman, M. Langevin, Y. Liu, J. Samaran, G. Misrachi, A. Nazaret, O.
936 Clivio, C. Xu, T. Ashuach, M. Gabitto, M. Lotfollahi, V. Svensson, E. da Veiga Beltrame,
937 V. Kleshchevnikov, C. Talavera-Lopez, L. Pachter, F. J. Theis, A. Streets, M. I. Jordan,
938 J. Regier, N. Yosef, A Python library for probabilistic analysis of single-cell omics data.
939 *Nat Biotechnol* **40**, 163-166 (2022).
940 77. J. D. Hunter, Matplotlib: A 2D graphics environment. *Computing in Science &*
941 *Engineering* **3**, 90-95 (2007).
942 78. H. Thorvaldsdottir, J. T. Robinson, J. P. Mesirov, Integrative Genomics Viewer (IGV):
943 high-performance genomics data visualization and exploration. *Brief Bioinform* **14**,
944 178-192 (2013).
945 79. M. J. Park, K. Chung, Endogenous lectin (RL-29) expression of the autonomic
946 preganglionic neurons in the rat spinal cord. The Anatomical Record 254, 54-60
947 (1999).
948 80. C. O. Miranda, K. Hegedus, H. Wildner, H. U. Zeilhofer, M. Antal, Morphological and
949 neurochemical characterization of glycinergic neurons in laminae I-IV of the mouse
950 spinal dorsal horn. J Comp Neurol 530, 607-626 (2022).
951 81. F. Guo, Y. Wang, TCF7l2, a nuclear marker that labels premyelinating
952 oligodendrocytes and promotes oligodendroglial lineage progression. Glia 71, 143-
953 154 (2023).
954 82. E. Weihe, C. Depboylu, B. Schutz, M. K. Schafer, L. E. Eiden, Three types of tyrosine
955 hydroxylase-positive CNS neurons distinguished by dopa decarboxylase and VMAT2
956 co-expression. Cell Mol Neurobiol 26, 659-678 (2006).
957 83. J. Sun, Y. Song, Z. Chen, J. Qiu, S. Zhu, L. Wu, L. Xing, Heterogeneity and Molecular
958 Markers for CNS Glial Cells Revealed by Single-Cell Transcriptomics. Cell Mol
959 Neurobiol 42, 2629-2642 (2022).
960 84. M. Dallaporta, M. S. Bonnet, K. Horner, J. Trouslard, A. Jean, J. D. Troadec, Glial cells
961 of the nucleus tractus solitarius as partners of the dorsal hindbrain regulation of
962 energy balance: a proposal for a working hypothesis. Brain Res 1350, 35-42 (2010).
963 85. J. Kalucka, L. de Rooij, J. Goveia, K. Rohlenova, S. J. Dumas, E. Meta, N. V.
964 Conchinha, F. Taverna, L. A. Teuwen, K. Veys, M. Garcia-Caballero, S. Khan, V.
965 Geldhof, L. Sokol, R. Chen, L. Treps, M. Borri, P. de Zeeuw, C. Dubois, T. K.
966 Karakach, K. D. Falkenberg, M. Parys, X. Yin, S. Vinckier, Y. Du, R. A. Fenton, L.
967 Schoonjans, M. Dewerchin, G. Eelen, B. Thienpont, L. Lin, L. Bolund, X. Li, Y. Luo, P.
968 Carmeliet, Single-Cell Transcriptome Atlas of Murine Endothelial Cells. Cell 180, 764-
969 779 e720 (2020).
970 86. N. Dani, R. H. Herbst, C. McCabe, G. S. Green, K. Kaiser, J. P. Head, J. Cui, F. B.
971 Shipley, A. Jang, D. Dionne, L. Nguyen, C. Rodman, S. J. Riesenfeld, J. Prochazka, M.
972 Prochazkova, R. Sedlacek, F. Zhang, V. Bryja, O. Rozenblatt-Rosen, N. Habib, A.
973 Regev, M. K. Lehtinen, A cellular and spatial map of the choroid plexus across brain
974 ventricles and ages. Cell 184, 3056-3074 e3021 (2021).
975 87. B. Ray, J. A. Bailey, S. Sarkar, D. K. Lahiri, Molecular and immunocytochemical
976 characterization of primary neuronal cultures from adult rat brain: Differential
977 expression of neuronal and glial protein markers. J Neurosci Methods 184, 294-302
978 (2009).
979 88. S. E. Lauri, M. Ryazantseva, E. Orav, A. Vesikansa, T. Taira, Kainate receptors in the
980 developing neuronal networks. Neuropharmacology 195, 108585 (2021).
981 89. Y. H. Song, J. Yoon, S. H. Lee, The role of neuropeptide somatostatin in the brain and
982 its application in treating neurological disorders. Exp Mol Med 53, 328-338 (2021).

90. H. W. Song, K. L. Foreman, B. D. Gastfriend, J. S. Kuo, S. P. Palecek, E. V. Shusta, Transcriptomic comparison of human and mouse brain microvessels. Sci Rep 10, 12358 (2020).
91. L. Xu, Y. Yao, Central Nervous System Fibroblast-Like Cells in Stroke and Other Neurological Disorders. Stroke 52, 2456-2464 (2021).
92. U. Ernsberger, H. Rohrer, Sympathetic tales: subdivisons of the autonomic nervous system and the impact of developmental studies. Neural Dev 13, 20 (2018).
93. C. R. Gajera, H. Emich, O. Lioubinski, A. Christ, R. Beckervordersandforth-Bonk, K. Yoshikawa, S. Bachmann, E. I. Christensen, M. Gotz, G. Kempermann, A. S. Peterson, T. E. Willnow, A. Hammes, LRP2 in ependymal cells regulates BMP signaling in the adult neurogenic niche. J Cell Sci 123, 1922-1930 (2010).
94. A. MacDonald, B. Lu, M. Caron, N. Caporicci-Dinucci, D. Hatrock, K. Petrecca, G. Bourque, J. A. Stratton, Single Cell Transcriptomics of Ependymal Cells Across Age, Region and Species Reveals Cilia-Related and Metal Ion Regulatory Roles as Major Conserved Ependymal Cell Functions. Front Cell Neurosci 15, 703951 (2021).
95. H. W. Jeong, R. Dieguez-Hurtado, H. Arf, J. Song, H. Park, K. Kruse, L. Sorokin, R. H. Adams, Single-cell transcriptomics reveals functionally specialized vascular endothelium in brain. Elife 11, (2022).
96. K. Huizer, D. A. M. Mustafa, J. C. Spelt, J. M. Kros, A. Sacchetti, Improving the characterization of endothelial progenitor cell subsets by an optimized FACS protocol. PLoS One 12, e0184895 (2017).
97. E. Gerrits, Y. Heng, E. Boddeke, B. J. L. Eggen, Transcriptional profiling of microglia; current state of the art and future perspectives. Glia 68, 740-755 (2020).
98. P. T. Shah, J. A. Stratton, M. G. Stykel, S. Abbasi, S. Sharma, K. A. Mayr, K. Koblinger, P. J. Whelan, J. Biernaskie, Single-Cell Transcriptomics and Fate Mapping of Ependymal Cells Reveals an Absence of Neural Stem Cell Function. Cell 173, 1045-1057 e1049 (2018).
99. C. G. Causing, A. Gloster, R. Aloyz, S. X. Bamji, E. Chang, J. Fawcett, G. Kuchel, F. D. Miller, Synaptic Innervation Density Is Regulated by Neuron-Derived BDNF. Neuron 18, 257–267 (1997).
100. Y. Zhang, S. A. Sloan, L. E. Clarke, C. Caneda, C. A. Plaza, P. D. Blumenthal, H. Vogel, G. K. Steinberg, M. S. Edwards, G. Li, J. A. Duncan, 3rd, S. H. Cheshier, L. M. Shuer, E. F. Chang, G. A. Grant, M. G. Gephart, B. A. Barres, Purification and Characterization of Progenitor and Mature Human Astrocytes Reveals Transcriptional and Functional Differences with Mouse. Neuron 89, 37-53 (2016).
101. F. Langlet, Tanycyte Gene Expression Dynamics in the Regulation of Energy Homeostasis. Front Endocrinol (Lausanne) 10, 286 (2019).
102. O. Uriarte Huarte, D. Kyriakis, T. Heurtaux, Y. Pires-Afonso, K. Grzyb, R. Halder, M. Buttini, A. Skupin, M. Mittelbronn, A. Michelucci, Single-Cell Transcriptomics and In Situ Morphological Analyses Reveal Microglia Heterogeneity Across the Nigrostriatal Pathway. Front Immunol 12, 639613 (2021).
103. R. E. Pepper, K. A. Pitman, C. L. Cullen, K. M. Young, How Do Cells of the Oligodendrocyte Lineage Affect Neuronal Circuits to Influence Motor Function, Memory and Mood? Front Cell Neurosci 12, 399 (2018).
104. A. Maegawa, K. Murata, K. Kuroda, S. Fujieda, Y. Fukazawa, Cellular Profiles of Prodynorphin and Preproenkephalin mRNA-Expressing Neurons in the Anterior Olfactory Tubercle of Mice. Front Neural Circuits 16, 908964 (2022).
105. S. T. Hentges, V. Otero-Corchon, R. L. Pennock, C. M. King, M. J. Low, Proopiomelanocortin expression in both GABA and glutamate neurons. J Neurosci 29, 13684-13690 (2009).
106. W. Sun, A. Cornwell, J. Li, S. Peng, M. J. Osorio, N. Aalling, S. Wang, A. Benraiss, N. Lou, S. A. Goldman, M. Nedergaard, SOX9 Is an Astrocyte-Specific Nuclear Marker in the Adult Brain Outside the Neurogenic Regions. J Neurosci 37, 4493-4507 (2017).
107. A. T. Lee, D. Vogt, J. L. Rubenstein, V. S. Sohal, A class of GABAergic neurons in the prefrontal cortex sends long-range projections to the nucleus accumbens and elicits acute avoidance behavior. J Neurosci 34, 11519-11525 (2014).

108. M. Vanlandewijck, L. He, M. A. Mae, J. Andrae, K. Ando, F. Del Gaudio, K. Nahar, T. Lebouvier, B. Lavina, L. Gouveia, Y. Sun, E. Raschperger, M. Rasanen, Y. Zarb, N. Mochizuki, A. Keller, U. Lendahl, C. Betsholtz, A molecular atlas of cell types and zonation in the brain vasculature. Nature 554, 475-480 (2018).
109. M. Carlen, K. Meletis, C. Goritz, V. Darsalia, E. Evergren, K. Tanigaki, M. Amendola, F. Barnabe-Heider, M. S. Yeung, L. Naldini, T. Honjo, Z. Kokaia, O. Shupliakov, R. M. Cassidy, O. Lindvall, J. Frisen, Forebrain ependymal cells are Notch-dependent and generate neuroblasts and astrocytes after stroke. Nat Neurosci 12, 259-267 (2009).
110. J. Garcia-Revilla, A. Boza-Serrano, A. M. Espinosa-Oliva, M. S. Soto, T. Deierborg, R. Ruiz, R. M. de Pablos, M. A. Burguillos, J. L. Venero, Galectin-3, a rising star in modulating microglia activation under conditions of neurodegeneration. Cell Death Dis 13, 628 (2022).
111. A. C. Yang, R. T. Vest, F. Kern, D. P. Lee, M. Agam, C. A. Maat, P. M. Losada, M. B. Chen, N. Schaum, N. Khoury, A. Toland, K. Calcuttawala, H. Shin, R. Palovics, A. Shin, E. Y. Wang, J. Luo, D. Gate, W. J. Schulz-Schaeffer, P. Chu, J. A. Siegenthaler, M. W. McNerney, A. Keller, T. Wyss-Coray, A human brain vascular atlas reveals diverse mediators of Alzheimer's risk. Nature 603, 885-892 (2022).
112. S. Chasseigneaux, Y. Moraca, V. Cochois-Guegan, A. C. Boulay, A. Gilbert, S. Le Crom, C. Blugeon, C. Firmo, S. Cisternino, J. L. Laplanche, E. Curis, X. Decleves, B. Saubamea, Isolation and differential transcriptome of vascular smooth muscle cells and mid-capillary pericytes from the rat brain. Sci Rep 8, 12272 (2018).
113. Z. Gao, K. Ure, J. L. Ables, D. C. Lagace, K. A. Nave, S. Goebbels, A. J. Eisch, J. Hsieh, Neurod1 is essential for the survival and maturation of adult-born neurons. Nat Neurosci 12, 1090-1092 (2009).
114. T. Kodama, S. Guerrero, M. Shin, S. Moghadam, M. Faulstich, S. du Lac, Neuronal classification and marker gene identification via single-cell expression profiling of brainstem vestibular neurons subserving cerebellar learning. J Neurosci 32, 7819-7831 (2012).
115. J. Manjarrez-Marmolejo, J. Franco-Pérez, Gap Junction Blockers- An Overview of their Effects on Induced Seizures in Animal Models. Current Neuropharmacology 14, 759-771 (2016).
116. T. Paretkar, E. Dimitrov, Activation of enkephalinergic (Enk) interneurons in the central amygdala (CeA) buffers the behavioral effects of persistent pain. Neurobiol Dis 124, 364-372 (2019).
117. Z. Zhang, Z. Ma, W. Zou, H. Guo, M. Liu, Y. Ma, L. Zhang, The Appropriate Marker for Astrocytes: Comparing the Distribution and Expression of Three Astrocytic Markers in Different Mouse Cerebral Regions. Biomed Res Int 2019, 9605265 (2019).
118. A. M. Jurga, M. Paleczna, J. Kadluczka, K. Z. Kuter, Beyond the GFAP-Astrocyte Protein Markers in the Brain. Biomolecules 11, (2021).
119. V. Dyachuk, A. Furlan, M. K. Shahidi, M. Giovenco, N. Kaukua, C. Konstantinidou, V. Pachnis, F. Memic, U. Marklund, T. Müller, C. Birchmeier, K. Fried, P. Ernfors, I. Adameyko, Parasympathetic neurons originate from nerve-associated peripheral glial progenitors. Science 345, 82-87 (2014).
120. M. S. Erwig, J. Patzig, A. M. Steyer, P. Dibaj, M. Heilmann, I. Heilmann, R. B. Jung, K. Kusch, W. Möbius, O. Jahn, K.-A. Nave, H. B. Werner, Anillin facilitates septin assembly to prevent pathological outfoldings of central nervous system myelin. eLife 8, (2019).
121. J. Spaas, W. M. A. Franssen, C. Keytsman, L. Blancquaert, T. Vanmierlo, J. Bogie, B. Broux, N. Hellings, J. van Horssen, D. K. Posa, D. Hoetker, S. P. Baba, W. Derave, B. O. Eijnde, Carnosine quenches the reactive carbonyl acrolein in the central nervous system and attenuates autoimmune neuroinflammation. J Neuroinflammation 18, 255 (2021).
122. J. DeSisto, R. O'Rourke, H. E. Jones, B. Pawlikowski, A. D. Malek, S. Bonney, F. Guimiot, K. L. Jones, J. A. Siegenthaler, Single-Cell Transcriptomic Analyses of the Developing Meninges Reveal Meningeal Fibroblast Diversity and Function. Dev Cell 54, 43-59 e44 (2020).

123. D. S. Liu, T. L. Xu, Cell-Type Identification in the Autonomic Nervous System. Neurosci Bull 35, 145-155 (2019).
124. B. J. Kang, D. A. Chang, D. D. Mackay, G. H. West, T. S. Moreira, A. C. Takakura, J. M. Gwilt, P. G. Guyenet, R. L. Stornetta, Central nervous system distribution of the transcription factor Phox2b in the adult rat. J Comp Neurol. 503, 627-641 (2007).
125. M. Adler, N. Moriel, A. Goeva, I. Avraham-Davidi, S. Mages, T. S. Adams, N. Kaminski, E. Z. Macosko, A. Regev, R. Medzhitov, M. Nitzan, Emergence of division of labor in tissues through cell interactions and spatial cues. Cell Rep 42, 112412 (2023).
126. A. Steimel, J. Suh, A. Hussainkhel, S. Deheshi, J. M. Grants, R. Zapf, D. G. Moerman, S. Taubert, H. Hutter, The C. elegans CDK8 Mediator module regulates axon guidance decisions in the ventral nerve cord and during dorsal axon navigation. Dev Biol 377, 385-398 (2013).
127. T. Daiber, C. J. VanderZwan-Butler, G. J. Bashaw, T. A. Evans, Conserved and divergent aspects of Robo receptor signaling and regulation between Drosophila Robo1 and C. elegans SAX-3. Genetics 217, (2021).
128. S. Schmetsdorf, U. Gärtner, T. Arendt, Constitutive Expression of Functionally Active Cyclin-Dependent Kinases and Their Binding Partners Suggests Noncanonical Functions of Cell Cycle Regulators in Differentiated Neurons. Cerebral Cortex 17, 1821–1829 (2007).
129. K. K. Kummer, M. Zeidler, T. Kalpachidou, M. Kress, Role of IL-6 in the regulation of neuronal development, survival and function. Cytokine 144, 155582 (2021).
130. P. März, J. G. Cheng, R. A. Gadient, P. H. Patterson, T. Stoyan, U. Otten, S. Rose-John, Sympathetic neurons can produce and respond to interleukin 6. Proc Natl Acad Sci 95, 3251-3256 (1998).
131. K. M. McGrail, J. M. Phillips, K. J. Sweadner, Immunofluorescent localization of three Na,K-ATPase isozymes in the rat central nervous system: both neurons and glia can express more than one Na,K-ATPase. J Neurosci 11, 381-391 (1991).
132. H. Poulsen, H. Khandelia, J. P. Morth, M. Bublitz, O. G. Mouritsen, J. Egebjerg, P. Nissen, Neurological disease mutations compromise a C-terminal ion pathway in the Na(+)/K(+)-ATPase. Nature 467, 99-102 (2010).
133. A. Abousaab, J. Warsi, B. Elvira, F. Lang, Caveolin-1 Sensitivity of Excitatory Amino Acid Transporters EAAT1, EAAT2, EAAT3, and EAAT4. J Membr Biol 249, 239-249 (2016).
134. E. R. Bongarzone, C. W. Campagnoni, K. Kampf, E. C. Jacobs, V. W. Handley, V. Schonmann, A. T. Campagnoni, Identification of a new exon in the myelin proteolipid protein gene encoding novel protein isoforms that are restricted to the somata of oligodendrocytes and neurons. J Neurosci 19, 8349-8357 (1999).
135. L. F. Nunnelly, M. Campbell, D. I. Lee, P. Dummer, G. Gu, V. Menon, E. Au, St18 specifies globus pallidus projection neuron identity in MGE lineage. Nat Commun 13, 7735 (2022).
136. C. Plachez, C. Lindwall, N. Sunn, M. Piper, R. X. Moldrich, C. E. Campbell, J. M. Osinski, R. M. Gronostajski, L. J. Richards, Nuclear factor I gene expression in the developing forebrain. J Comp Neurol 508, 385-401 (2008).
137. J. Fraser, A. Essebier, A. S. Brown, R. A. Davila, D. Harkins, O. Zalucki, L. P. Shapiro, P. Penzes, B. J. Wainwright, M. P. Scott, R. M. Gronostajski, M. Boden, M. Piper, T. J. Harvey, Common Regulatory Targets of NFIA, NFIX and NFIB during Postnatal Cerebellar Development. Cerebellum 19, 89-101 (2020).
138. L. Dubois , A. Vincent, The COE--Collier/Olf1/EBF--transcription factors: structural conservation and diversity of developmental functions. 108 3-12, (2001).
139. Y. Liu, T. Lear, O. Iannone, S. Shiva, C. Corey, S. Rajbhandari, J. Jerome, B. B. Chen, R. K. Mallampalli, The Proapoptotic F-box Protein Fbxl7 Regulates Mitochondrial Function by Mediating the Ubiquitylation and Proteasomal Degradation of Survivin. J Biol Chem 290, 11843-11852 (2015).
140. H. Kim, N. C. Berens, N. E. Ochandarena, B. D. Philpot, Region and Cell Type Distribution of TCF4 in the Postnatal Mouse Brain. Front Neuroanat 14, 42 (2020).
141. A. Sirp, A. Shubina, J. Tuvikene, L. Tamberg, C. S. Kiir, L. Kranich, T. Timmusk, Expression of alternative transcription factor 4 mRNAs and protein isoforms in the

1152 developing and adult rodent and human tissues. Front Mol Neurosci 15, 1033224
1153 (2022).
1154 142. R. D. Hodge, T. E. Bakken, J. A. Miller, K. A. Smith, E. R. Barkan, L. T. Graybuck, J. L.
1155 Close, B. Long, N. Johansen, O. Penn, Z. Yao, J. Eggermont, T. Hollt, B. P. Levi, S. I.
1156 Shehata, B. Aevermann, A. Beller, D. Bertagnolli, K. Brouner, T. Casper, C. Cobbs, R.
1157 Dalley, N. Dee, S. L. Ding, R. G. Ellenbogen, O. Fong, E. Garren, J. Goldy, R. P.
1158 Gwinn, D. Hirschstein, C. D. Keene, M. Keshk, A. L. Ko, K. Lathia, A. Mahfouz, Z.
1159 Maltzer, M. McGraw, T. N. Nguyen, J. Nyhus, J. G. Ojemann, A. Oldre, S. Parry, S.
1160 Reynolds, C. Rimorin, N. V. Shapovalova, S. Somasundaram, A. Szafer, E. R.
1161 Thomsen, M. Tieu, G. Quon, R. H. Scheuermann, R. Yuste, S. M. Sunkin, B. Lelieveldt,
1162 D. Feng, L. Ng, A. Bernard, M. Hawrylycz, J. W. Phillips, B. Tasic, H. Zeng, A. R.
1163 Jones, C. Koch, E. S. Lein, Conserved cell types with divergent features in human
1164 versus mouse cortex. Nature 573, 61-68 (2019).
1165 143. T. Kuroda, S. Yasuda, S. Tachi, S. Matsuyama, S. Kusakawa, K. Tano, T. Miura, A.
1166 Matsuyama, Y. Sato, SALL3 expression balance underlies lineage biases in human
1167 induced pluripotent stem cell differentiation. Nat Commun 10, 2175 (2019).
1168 144. F. Morello, D. Borshagovski, M. Survila, L. Tikker, S. Sadik-Ogli, A. Kirjavainen, N.
1169 Estartus, L. Knaapi, L. Lahti, P. Toronen, L. Mazutis, A. Delogu, M. Salminen, K.
1170 Achim, J. Partanen, Molecular Fingerprint and Developmental Regulation of the
1171 Tegmental GABAergic and Glutamatergic Neurons Derived from the Anterior
1172 Hindbrain. Cell Rep 33, 108268 (2020).
1173 145. L. Wolf, C. S. Gao, K. Gueta, Q. Xie, T. Chevallier, N. R. Podduturi, J. Sun, I. Conte, P.
1174 S. Zelenka, R. Ashery-Padan, J. Zavadil, A. Cvekl, Identification and characterization
1175 of FGF2-dependent mRNA: microRNA networks during lens fiber cell differentiation.
1176 G3 (Bethesda) 3, 2239-2255 (2013).
1177 146. H. Liu, M. Aramaki, Y. Fu, D. Forrest, Retinoid-Related Orphan Receptor beta and
1178 Transcriptional Control of Neuronal Differentiation. Curr Top Dev Biol 125, 227-255
1179 (2017).
1180 147. M. G. Del Barrio, S. Bourane, K. Grossmann, R. Schule, S. Britsch, D. D. O'Leary, M.
1181 Goulding, A transcription factor code defines nine sensory interneuron subtypes in the
1182 mechanosensory area of the spinal cord. PLoS One 8, e77928 (2013).
1183 148. Y. Li, A. Osuma, E. Correa, M. A. Okebalama, P. Dao, O. Gaylord, J. Aburas, P. Islam,
1184 A. E. Brown, P. Kratsios, Establishment and maintenance of motor neuron identity via
1185 temporal modularity in terminal selector function. Elife 9, (2020).
1186 149. D. Moruzzo, L. Nobbio, B. Sterlini, G. G. Consalez, F. Benfenati, A. Schenone, A.
1187 Corradi, The Transcription Factors EBF1 and EBF2 Are Positive Regulators of
1188 Myelination in Schwann Cells. Mol Neurobiol 54, 8117-8127 (2017).
1189 150. M. A. Jimenez, P. Akerblad, M. Sigvardsson, E. D. Rosen, Critical role for Ebf1 and
1190 Ebf2 in the adipogenic transcriptional cascade. Mol Cell Biol 27, 743-757 (2007).
1191 151. H. Yu, M. Rubinstein, M. J. Low, Developmental single-cell transcriptomics of
1192 hypothalamic POMC neurons reveal the genetic trajectories of multiple
1193 neuropeptidergic phenotypes. Elife 11, (2022).
1194 152. I. Singh, L. Wang, B. Xia, J. Liu, A. Tahiri, A. El Ouaamari, M. B. Wheeler, Z. P. Pang,
1195 Activation of arcuate nucleus glucagon-like peptide-1 receptor-expressing neurons
1196 suppresses food intake. Cell Biosci 12, 178 (2022).
1197 153. L. Xiao, D. P. Merullo, T. M. I. Koch, M. Cao, M. Co, A. Kulkarni, G. Konopka, T. F.
1198 Roberts, Expression of FoxP2 in the basal ganglia regulates vocal motor sequences in
1199 the adult songbird. Nat Commun 12, 2617 (2021).
1200 154. T. T. Du, J. B. Dewey, E. L. Wagner, R. Cui, J. Heo, J. J. Park, S. P. Francis, E. Perez-
1201 Reyes, S. J. Guillot, N. E. Sherman, W. Xu, J. S. Oghalai, B. Kachar, J. B. Shin, LMO7
1202 deficiency reveals the significance of the cuticular plate for hearing function. Nat
1203 Commun 10, 1117 (2019).
1204 155. M. A. Wozniak, B. M. Baker, C. S. Chen, K. L. Wilson, The emerin-binding transcription
1205 factor Lmo7 is regulated by association with p130Cas at focal adhesions. PeerJ 1,
1206 e134 (2013).
1207 156. T. Kawaue, A. Shitamukai, A. Nagasaka, Y. Tsunekawa, T. Shinoda, K. Saito, R.
1208 Terada, M. Bilgic, T. Miyata, F. Matsuzaki, A. Kawaguchi, Lzts1 controls both neuronal

delamination and outer radial glial-like cell generation during mammalian cerebral development. Nat Commun 10, 2780 (2019).
157. O. Randlett, L. Poggi, F. R. Zolessi, W. A. Harris, The oriented emergence of axons from retinal ganglion cells is directed by laminin contact in vivo. Neuron 70, 266-280 (2011).
158. N. Ichikawa-Tomikawa, J. Ogawa, V. Douet, Z. Xu, Y. Kamikubo, T. Sakurai, S. Kohsaka, H. Chiba, N. Hattori, Y. Yamada, E. Arikawa-Hirasawa, Laminin alpha1 is essential for mouse cerebellar development. Matrix Biol 31, 17-28 (2012).
159. E. S. Liau, S. Jin, Y. C. Chen, W. S. Liu, M. Calon, S. Nedelec, Q. Nie, J. A. Chen, Single-cell transcriptomic analysis reveals diversity within mammalian spinal motor neurons. Nat Commun 14, 46 (2023).

Acknowledgements

We would like to thank authors of the Ludwig and the Dowsett publications for making publicly available their datasets. We thank M. Myers Jr. for the valuable help provided; S. Hebert and S. Bailey for their insights and suggestions in regards to the bioinformatic analysis; members of the Kokoeva lab for their insights on the *in-situ* hybridization and immunohistochemistry pipelines; S. Feng and M. Fu for technical assistance for images acquisition at the Molecular Imaging Platform at the RI-MUHC, and A. Duensing for assistance with relevant file transfer.

Funding

This research was also supported by grants from Canadian Institutes for Health Research (PJT180590 for PVS and 202010PJT for MK) the Natural Sciences and Engineering Research Council of Canada (RGPIN-2022-03390). HJM was funded in part by the Canada First Research Excellence Fund and Fonds de recherche du Quebec, awarded to the Healthy Brains, Healthy Lives initiative.

Author contributions

Conceptualization: CH and PS
Methodology: CH, AB, LM, MK and PS
Sample collection: AB and PS
Software: CH, LM and HJM
Data analysis: CH, LM, MK and PS
Data curation: CH and HJM
Validation of findings: CH, FS, HJM and PS
Imaging: CH and PS
Visualization: CH, MK and PS
Supervision: CH and PS
Writing—original draft: CH and PS —review and editing: CH, AB, LM, FS, HJM, MK and PS
Funding acquisition: MK and PS

Competing interests

The authors declare that they have no competing interests.

Data and materials availability

All data needed to evaluate the conclusions in the paper are present in the paper and/or the Supplementary Materials. FASTQ files have been deposited in the NCBI Sequence Read Archive (Accession: PRJNA1161292). In addition, our murine and rat datasets have been made available for visualization and analysis through the Broad Institute Single Cell Portal (https://singlecell.broadinstitute.org/single_cell/study/SCP2773). The labels from our cell atlas can be transferred to new datasets through treeArches using the available hosted Jupyter Notebook in Google Colab for the mouse data (https://colab.research.google.com/drive/1v983gcQxIwBN-4lGx18JXPweZoKqMbwX#scrollTo=SJTZppZWa-63), and for the rodent data (https://colab.research.google.com/drive/10tAmfRosMscuBak6wHX80TgdEBsHeWQB#scrollTo=941ab5c1-8910-4e67-a632-4d18601d45b4). Original code used for constructing the murine and rodent cell hierarchies and predicting labels using treeArches are available in the GitHub repository https://github.com/LabSabatini/DVC_cell_atlas.

Figure legends

Figure 1: Two layers of cell identity for the murine DVC cells from snRNA-seq data

A. Adult C57BL/6J mice were subjected to 10X Genomics-based snRNA barcoding and sequencing after dissection of their DVC (n=30). **B.** Labeled UMAP plot of the mouse DVC (cells n=99,740) at the lowest resolution (layer 1) including 4 cell identities, and **C.** the cell class (layer 2) including 18. **D.** Heatmap of the main marker genes (average log2FC expression >80 percentiles of upregulated genes) for each neuronal class of the mouse DVC (MAST algorithm; neurons n= 48,131; adj. p<0.05). Each column is one cell and each row is one marker gene. **E.** Stacked barplot of log-normalized counts of genes for 10 transcripts (i.e. *Gad2*, *Gad1*, *Slc6a5*, *Slc17a6*, *Slc18a2*, *Addc*, *Sst*, *Npy*, *Cck* and *Slc5a7*) related to transmission/release of 8 neurotransmitters and neuropeptides, by neuronal cell class. Each bar represents one neuron (n=48,131).

snRNA-seq=single-nuclei RNA-sequencing; DVC=dorsal vagal complex; FACs=fluorescence-activated cell sorting; UMAP=uniform manifold approximation and projection; FC=fold-change; adj.=adjusted; GABA=gamma-aminobutyric acid

Figure 2: Third layer of non-neuronal murine DVC cell identities

A. Labeled UMAP plot of the mouse DVC with the 15 non-neuronal cell identities shown (total cells n=99,740; non-neuronal cells n=51,609). **B.** UMAP plot showing scaled expression of *Gfap*, *Gria2* and *Kcnj3* genes in Ca^+-permeable astrocytes (circled; total cells n=99,740; Ca^+-permeable astrocytes n=1,719). **C.** Barplot of log-normalized expression of six genes in oligodendrocytes (premyelinating n=267; myelinating intermediate n=25,692; myelinating n= 6,170). Only premyelinating oligodendrocytes lack expression of *Mobp*, involved in myelin formation. Reduction of *Synpr* and *Opalin* expression is observed as *Anln* and *Aff3* increase in myelinating oligodendrocytes. **D.** Balloon plot of the main cell types of non-neuronal cells and neurons showing average log-normalized counts of their marker genes (MAST algorithm; adj. p<0.05). Markers shown are upregulated genes in >80% of cells per group with average log2FC>4, or upregulated in >70% of cells with average log2FC>8.

DVC=dorsal vagal complex; UMAP=uniform manifold approximation and projection; APNTS=Area postrema and nucleus of the solitary tract; OL=oligodendrocyte; OPC=oligodendrocyte precursor cell; Smc=smooth muscle cells

Figure 3: Neuronal populations of the murine DVC

A. Labeled UMAP plot with the neuronal layer 3 cell identities (neurons n=48,131). **B.** Monoamine class balloon plot showing average log-normalized expression of marker

genes for each cell identity (MAST algorithm; M0 cells n=770, M1 cells n=551, M2 cells n=666 and M3 cells n=2,593; adj. $p<0.05$), and **C.** heatmap of expression of monoamine related genes. In the heatmap, each column represents one cell and each row, one gene. **D.** Barplot of *Gcg* average log-normalized expression by neuronal cell identity. **E.** UMAP plot showing the expression of leptin receptor and prolactin receptor genes in neurons. The GLP1 cluster is highlighted (GLP1 cells n=153). **F.** Stacked barplot of the proportion of cells expressing one or more GABA-related genes (i.e. *Slc32a1*, *Gad1*, *Gad2*) and glutamate-related genes (i.e. *Slc17a6*, *Slc17a7*). The proportion of cells per cell group co-expressing GABA and glutamate associated genes are shown in purple. Only cells with log-normalized counts >0 were considered to express the genes.

DVC=dorsal vagal complex; UMAP=uniform manifold approximation and projection; Res.=resolution; GABA=gamma-aminobutyric acid

Figure 4: *Th* and *Cck* co-expression in the DVC

A. UMAP plot of neuronal *Th* and *Cck* scaled expression and cells with co-expression of both genes (neurons n=48,131; *Th*-expressing neurons n=764; *Cck*-expressing neurons n=3,821; *Th*/*Cck* co-expressing neurons n=80). On the right plot, cells highlighted in magenta are the co-expressing neurons. The three neuronal cell identities in which the majority of nuclear co-expression of *Th* and *Cck* mRNA is found, as well as the percentage of total co-expressing neurons, are shown. **B.** *In-situ* hybridization of *Cck* and *Th* mRNA in coronal mouse DVC sections corresponding to -7.2mm and -7.56mm relative to bregma showing overlap of *Th*/*Cck*. Some of the cells with overlapping signal are highlighted with an arrow in the enhanced merged image.

DVC=dorsal vagal complex; UMAP=uniform manifold approximation and projection

Figure 5: The murine DVC cell hierarchy

A. Dendrogram of the harmonized hierarchy which incorporates cells from Ludwig and our datasets. Orange cell identities are a fourth layer of cell identity resolution obtained as some of the Ludwig dataset identities are subgroups of our original cell identities at their highest resolution. Magenta labels represent layer 3 of cellular granularity. These two layers are considered high-resolution. **B.** UMAP plot of the integration between our and Ludwig datasets using treeArches (cells n=171,868). **C.** Pairwise heatmap showing the proportion of cells originally labeled in this study and in Ludwig dataset (y-axis), predicted to belong to each identity group (x-axis) by treeArches using our learned harmonized hierarchy. In blue are the labels considered non-specific for a high-resolution cell identity (n=2,324; 1.3%). In pink are the cell labels for rejected cells, therefore not assigned any identity by treeArches (n=3,108; 1.8%).

1344 D. UMAP plot of the Dowsett dataset labeled through treeArches using the learned
1345 harmonized hierarchy representation from our murine DVC atlas. The 'unlabeled' cells
1346 include those rejected by the algorithm and thus without an assigned identity, and
1347 those with an unspecific layer-3/4 label. For example, some were labeled 'neuron' or
1348 'monoamine-class' but without a high-resolution cell identity.
1349 UMAP=uniform manifold approximation and projection; APNTS=Area postrema and nucleus of the
1350 solitary tract; Lnc=long non-coding; OL=oligodendrocyte; OPC=oligodendrocyte precursor cell;
1351 Neur=neuronal; COE=collier/Olf1/EBF transcription factor
1352

1353 **Figure 6: The snRNA-seq derived cell identities for the rat DVC**

1354 A. Schematic of the pipeline for snRNA-seq of the rat DVC. B. Labeled UMAP plots of
1355 the low resolution (i.e. layers 1 and 2 of granularity) and C. high resolution (i.e. layer
1356 3) cell identities in our rat DVC dataset (cells n=12,167). We labeled four layer-1,
1357 nineteen layer-2 and fifty-two layer-3 cell identities. Those labels novel to this dataset
1358 and not present in the murine data are highlighted with a pink ♦ symbol. We found a
1359 small cluster (cells n=35) that we could not corroborate its identity at any layer of
1360 cellular granularity that we named 'unspecific'.
1361 snRNA-seq=single-nuclei RNA-sequencing; DVC=dorsal vagal complex; FACs=fluorescence-
1362 activated cell sorting; UMAP=uniform manifold approximation and projection; APNTS=Area postrema
1363 and nucleus of the solitary tract; Lnc=long non-coding; OL=oligodendrocyte; OPC=cursor cell;
1364 Neur=neuronal; COE=collier/Olf1/EBF transcription factors
1365

1366 **Figure 7: Two novel neuronal classes specific to the rat DVC**

1367 A. Balloon plots comparing the expression of the marker genes of the two novel
1368 neuronal classes found in rats (cells n=12,167): immunity-akin and the ortus-akin
1369 classes (framed in gray). Expression is shown across the layer-2 rat cell identities.
1370 Based on the expression of two DVC neuronal markers *Mtus2* and *Syt1*, we
1371 corroborated those cell classes contain neurons, and not microglial or
1372 vascular/endothelial cells (In orange and red, respectively). The immunity-akin class
1373 (n=48 neurons) shares high expression of *Cst3*, *Inpp5d*, *Csf1r*, *Slco2b1* and *Lyn* with
1374 microglial cells. Meanwhile, the ortus-akin class (n=34 neurons) shows higher overlap
1375 of gene expression markers (i.e. *Arhgap31*, *Pdgfra*, *Bcas1*, *Ppfibp1* and *Itga9*) with
1376 OPCs (highlighted with a ♦ symbol). Mouse cell identities (cells n=99,740) do not
1377 show these expression patterns (framed in black). Average expression was calculated
1378 using log-normalized counts. B. Violin plots of scaled expression of 10 genes (i.e.
1379 *Glp1r, Gfral, Calcr, Ramp3, Gipr, Lepr, Cckar, Cckbr ,Mc4r* and *Prlr*) coding for
1380 metabolism-associated receptors in the Pdgfra and immunity-related rat neurons
1381 (Pdgfra neurons n=34; immunity-related neurons n=48). Pdgfra neurons are the only

1382 layer-3 identity within the ortus-akin class. An overlapping dotplot shows one dot per
1383 cell. **C.** Immunofluorescent detection of PDGFRA in mouse and rat DVC. Pink
1384 arrowheads point to cells with OPC morphology, white arrowheads point to cells with
1385 fibroblast morphology and the yellow arrowhead points to cells with neural
1386 morphology. **D.** Co-staining for PDGFRA and HuC/D in rat DVC with high
1387 magnification (right images) of area postrema PDGFRA-expressing cells . Yellow
1388 arrowheads indicate colocalization of HuC/D and PDGFRA.
1389 DVC=dorsal vagal complex; OPC=oligodendrocyte precursor cell; AP=area postrema; NTS=nucleus
1390 of the solitary tract; PDGFRA= Platelet-derived growth factor receptor A; CC=central canal
1391

1392 **Figure 8: The rodent DVC cell hierarchy**

1393 **A.** UMAP plot of the integration between the murine hierarchy and our rat dataset using
1394 treeArches (cells n=184,035). **B.** Dendrogram of the harmonized hierarchy of our
1395 labeled rat dataset and the murine DVC hierarchy. We highlight the incorporated rat
1396 cell identities (blue and magenta). Those in magenta are the novel rat identities
1397 established by us. The immunity-akin and the ortus-akin classes were not found in the
1398 murine datasets. The M3 and M5 rat identities are subgroups of a Ludwig layer 4 cell
1399 identity, therefore yields a fifth layer within the monoamine neuronal class.
1400 UMAP=uniform manifold approximation and projection; DVC=dorsal vagal complex; APNTS=Area
1401 postrema and nucleus of the solitary tract; Lnc=long non-coding; OL=oligodendrocyte;
1402 OPC=oligodendrocyte precursor cell; Neur=neuronal; COE=collier/Olf1/EBF transcription factors
1403

1404 **Figure 9: Meal-related transcriptional changes in the mouse DVC**

1405 **A.** Horizontal barplots of the number of differential genes between refed and ad libitum
1406 fed, and refed and fasted mice in glial cells and neurons per layer-2 cell identity (MAST
1407 algorithm on log-normalized counts; adj. $p<0.05$; refed neurons n=14,396; refed glial
1408 cells n=18,019; ad libitum fed neurons n= 9,885; ad libitum fed glial cells n=4,610;
1409 fasted neurons n=8,829; fasted glial cells n=12,496). **B.** Venn Diagrams of the
1410 differentially expressed genes in magnaclass 1 and magnaclass 2 neurons between
1411 refed and ad libitum fed, and between refed and fasted treatments (MAST algorithm
1412 on log-normalized counts). The number of overlapping log2FC≥1 upregulated genes
1413 between the two magnaclasses per treatment are highlighted. The treatment-induced
1414 changes in only one cell class are shown as non-overlapping. The percentage is
1415 based on the total differential genes surveyed per comparison. **C.** Volcano plots of the
1416 differential genes in neurons belonging to the magnaclass 1 and the magnaclass 2
1417 between refed and ad libitum fed, and **D.** refed and fasted treatments (MAST algorithm
1418 on log-normalized counts; adj. $p<0.05$). Each point represents one gene. Only genes
1419 upregulated or downregulated with a log2FC≥2 are labeled. Since we considered a

1420 minimum log fold-change of 0.1 between treatments per cell group, those genes with
1421 very low variance (i.e. log fold-change<0.1) were excluded from the differential
1422 expression analysis, therefore a variable number of genes are shown per comparison
1423 per identity, in the volcano plots.
1424 DVC=dorsal vagal complex; vr=versus; OPC=oligodendrocyte precursor cell; FC=fold-change;
1425 adj.=adjusted; NS=non-significant
1426

Supplementary Files

Figure S1: Mapping of *Gad2* and VGLUT2 in neurons

UMAP plot of the murine neurons (n=48,131) showing scaled log-normalized expression of **A.** *Gad2*, a gene related to GABA synthesis and transmission, **B.** and VGLUT2, a glutamate transporter. Cells with higher expression of *Gad2* belong to the neuronal magnaclass1, while cells with higher expression of VGLUT2 (*Slc17a6*) to the magnaclass2 (both highlighted in yellow in adjacent plots). However, the expression is not mutually exclusive among both classes, nor every neuron belonging to each class express the respective transcript.

UMAP=uniform manifold approximation and projection; GABA=gamma-aminobutyric acid; VGLUT2=vesicular glutamate transporter-2

Figure S2: Mapping of DVC populations in a murine hypothalamic dataset

UMAP plots of a randomly selected subset of the HypoMap database (cells n=76,260; samples n=32) labeled **A.** by sample and **B.** by original curated cell class. **C.** Balloon plot showing average expression of the top 5 upregulated gene markers of each neuronal DVC class (MAST algorithm; adj. $p<0.05$) in the neurons of the HypoMap subset (n=45,679). We selected the neuronal curated class cells from our initial HypoMap subset and reprocessed them, including clustering through *k*-nearest neighbors algorithm using the first 30 PCs and Harmony reduction embeddings. Resulting clusters at resolution 0.5 are shown. Average expression in the HypoMap neurons was calculated using log-normalized counts. **D.** Set of UMAP plots showing scaled expression of three genes (i.e. *Gfap*, *Gria2* and *Kcnj3*) which have a specific pattern of expression in murine DVC Ca^+-permeable astrocytes. The astrocytic population is circled in purple (astrocytes n=7,629) and while *Gfap* and *Gria2* expression is in agreement to what we observe in Ca^+-permeable astrocytes, in the hypothalamic astrocytes *Kcnj3* is not expressed. **E.** Set of UMAP plots of expression of *Aldh1a1* and *Stk39* which are markers of p-fibroblasts and s-fibroblasts in the DVC. The hypothalamic fibroblasts are circled in magenta (fibroblasts n=300).

DVC=dorsal vagal complex; UMAP=uniform manifold approximation and projection; AMPAr=α-amino-3-hydroxy-5-methyl-4-isoxazolepropionic acid receptor; GIRK1=G protein-coupled inwardly rectifying potassium channel 1; OPC=Oligodendrocyte precursor cell; NG=*Ng2* glial cell

Figure S3: Mapping of DVC astrocytes in a murine cortical/hippocampal dataset

UMAP plots of a cortical/hippocampal astrocytes dataset by **A.** sample, **B.** brain area and **C.** original astrocyte type (cell n=1,811). **D.** Set of UMAP plots showing scaled expression of three genes (i.e. *Gfap, Gria2* and *Kcnj3*) which have a specific pattern of expression in murine DVC Ca^+-permeable astrocytes. There is some overlap in *Gfap* and *Gria2* expression and almost no expression of *Kcnj3*, different from what we observe in DVC Ca^+-permeable astrocytes.

1465 Figure S4: Trajectory inference of the oligodendrocyte lineage
1466 Dotplot of the two principal components obtained through dimensionality reduction using the
1467 main 50 principal components analysis on log-normalized gene expression data in
1468 oligodendrocytes (cells n=32,129) **A.** merged and **B.** by sample, and on Harmony embeddings
1469 in oligodendrocytes **C.** merged and **D.** by sample. Cellular trajectory was inferred using
1470 SCORPIUS also on normalized gene expression data (**A.** and **B.**) and on the Harmony
1471 embeddings (**C.** and **D.**), and drawn across the data points (black line). Each data point
1472 represents one cell.
1473 OL=oligodendrocyte
1474
1475 Figure S5: Murine DVC clusters
1476 **A.** UMAP plot of the mouse DVC clusters at resolution 1 (cells n=99,740). Cells from mice
1477 exposed to 5 food and aversion-related treatments were integrated using the Harmony
1478 algorithm in R and the resulting embeddings were used to calculate the clusters and UMAP
1479 projections. We subset and re-clustered three clusters containing oligodendrocytes, vascular
1480 cells and fibroblasts, respectively (highlighted). **B.** Violin plots of the two types of fibroblasts in
1481 cluster 26, distinguished by *Skt39* (stress-response 's-fibroblasts') and *Aldh1a1* (perivascular
1482 'p-fibroblasts') expression. Each data point represents one cell (s-fibroblasts n=244; p-
1483 fibroblasts n=559). **C.** UMAP plot of subclusters from clusters 23 (oligodendrocytes) and **D.** 27
1484 (vascular cells) using the Harmony embeddings. Gene expression markers for cell populations
1485 were mapped (**Table S2**) and the smallest resolution that allowed to separate them was further
1486 used to label the cells. Cells in subclusters 1 and 2 from cluster 23 were labeled
1487 'premyelinating_OL' whilst subclusters 0 and 3 were labeled 'myelinating_intermediate_OL'. In
1488 cluster 27, subcluster 7 was labeled 'pericyte', subcluster 4 was labeled 'smooth_muscle' and
1489 the rest of the clusters were considered to be endothelial cells.
1490 DVC=dorsal vagal complex; Res.=resolution; UMAP=uniform manifold approximation and projection;
1491 OL=oligodendrocyte; smc=smooth muscle cell.
1492
1493 Figure S6: Mapping of markers for reactive microglia
1494 UMAP plot of the microglia from the mouse DVC showing scaled log-normalized expression of
1495 *Cd5*, *Zbp1*, *Cxcl9* and *Cxcl10*. Microglia was subset and re-processed using the harmony
1496 integration embeddings to obtain the UMAP coordinates (n=2,787).
1497 UMAP=uniform manifold approximation and projection; DVC=dorsal vagal complex
1498
1499 Figure S7: Initial murine cell hierarchy using our samples
1500 **A.** UMAP plot of the integration of our samples (based on the five mouse treatments
1501 administered to mice prior to euthanasia; see **Methods**) using treeArches. There were two
1502 cohorts of refed mice. **B.** UMAP plot of the fifty layer-3 cell identities obtained using the

1503 treeArches pipeline. **C.** Dendrogram showing the initial hierarchy of the three layers of cell
1504 identity established by us in this study.
1505 UMAP=uniform manifold approximation and projection; inj.=injected; APNTS=Area postrema and nucleus of the
1506 solitary tract; Lnc=long non-coding; OL=oligodendrocyte; OPC=oligodendrocyte precursor cell;
1507 COE=collier/Olf1/EBF transcription factors
1508

1509 Figure S8: Incorporation of the Ludwig dataset to our initial hierarchy using treeArches
1510 **A.** Barplot of log-normalized expression of OPC markers (i.e. *Pdgfra*, *Cspg4*, *C1ql1*) and
1511 premyelinating OL markers (i.e. *Bmp4*, *Fyn*) in the OPCs-labeled cells from the Ludwig dataset
1512 (total cells n=1,770; cells expressing >1 marker gene n=1,104). Cells labeled as OPCs in the
1513 Ludwig dataset are a mix of OPC and premyelinating OL. Some cells lack expression of the
1514 five marker genes used in this plot, they are represented on the left side with an empty bar and
1515 those expressing *Fyn*/*Bmp4* but not expressing the OPC markers are likely premyelinating OLs.
1516 Cells were ordered using hierarchical clustering based on these five gene expression data
1517 through the Ward's method in R. We only indicate the 'likely cell identity' for cells with
1518 expression of the five marker genes. **B.** UMAP showing the manual mapping of Ludwig and
1519 Dowsett neuronal clusters and identities in neurons from this study. We used the gene
1520 expression markers for all clusters from Ludwig and Dowsett to identify which of our neurons
1521 shared identity with those described in both publications. Only groups and clusters
1522 successfully mapped manually are shown. The Ludwig identities are in black, Dowsett
1523 identities are in blue and our identities are in purple. Most of neuronal clusters in both publicly
1524 available datasets, are subgroups of our cell identities.
1525 OPC=oligodendrocyte precursor cell; OL=oligodendrocyte; UMAP=uniform manifold approximation and
1526 projection; APNTS=Area postrema and nucleus of the solitary tract; Lnc=long non-coding; COE=collier/Olf1/EBF
1527 transcription factors
1528

1529 Figure S9: Rat DVC neurons
1530 **A.** Labeled UMAP plot with the neuronal layer 3 cell identities in our rat dataset (neurons
1531 n=4,721). Neurons were subset and re-processed to obtain the UMAP coordinates. **B.** Violin
1532 plots of scaled expression of 12 genes (i.e. *Gad2, Gad1, Slc6a5, Slc17a7, Slc17a6, Th, Ddc,*
1533 *Nos1, Sst, Npy, Cck* and *Slc5a7*) related to transmission/release of GABA, glutamate,
1534 monoamines, nitric oxide, somatostatin, neuropeptide-Y, cholecystokinin and acetylcholine in
1535 the Pdgfra and immunity-related rat neurons (Pdgfra neurons n=34; immunity-related neurons
1536 n=48). An overlapping dotplot shows one data point representing each cell.
1537 DVC=dorsal vagal complex; UMAP=uniform manifold approximation and projection; COE=collier/Olf1/EBF
1538 transcription factors; Lnc=long non-coding; GABA=gamma-aminobutyric acid
1539

Figure S10: Dendrogram after incorporation of the rat dataset to the murine hierarchy

Dendrogram (i.e. tree) resulting from incorporating our rat dataset (cells n=12,167) to the existing murine DVC cell hierarchy using treeArches. The rat cell populations in red that did not show similarity with the previously existing murine identities are appended at the bottom by treeArches (shown in red).

Figure S11: Expression of *Agrp* and *Hcrt* in DVC neurons

A. UMAP plots of the neurons (n=48,131) from our murine DVC dataset showing scaled expression of *Agrp* and *Hcrt*. **B.** *In-situ* hybridization images of *Agrp* and *Hcrt* in the DVC show no exonic mRNA. We included tissue sections of the arcuate nucleus of the hypothalamus and in the lateral hypothalamus as controls, and *Agrp* and *Hcrt* were present in these sites, respectively. For each reaction, tissue from the same mouse was used through two different sections, one including the DVC and one including the hypothalamic region. **C.** UMAP plots of the Dowsett (n=8,288) and the Ludwig datasets neurons (n=49,392) showing scaled expression of *Agrp* and *Hcrt*. **D.** Genome visualization of reads coverage in the *Agrp* and *Hcrt* regions of the *Mus musculus* refdata-gex-mm10-2020-A reference from two of our mouse sample sequencing replicates. Resulting BAM files from the original murine DVC FASTQ files were obtained after processing. We visualized the reads from these BAM files that mapped to the *Agrp* and *Hcrt* genes using IGV v2.16.1(*78*). The coverage of these genes (*Agrp* region: chr8:105,566,180–105,582,268; *Hcrt* region: chr11:100,761,693–100,762,931) are shown in gray. The majority of the reads mapped to the intronic regions of *Agrp*, and to the last part of the 3'-end of exon 2 and the 3'-untranslated region of *Hcrt*. **E.** UMAP plot of rat DVC neurons (n=4,721) showing scaled expression of *Agrp* and *Hcrt*. For all UMAP projections, neurons from each dataset were subset based on our labeling for our murine and rat datasets, the treeArches resulting labeling for the Dowsett dataset, and the original labeling from Ludwig and collaborators. Then the neurons were processed using Seurat(*63*) and integrated using Harmony(*65*), to yield the final UMAP embeddings.

DVC=dorsal vagal complex; UMAP=uniform manifold approximation and projection; AP=area postrema; NTS=nucleus of the solitary tract; ARH=arcuate nucleus of the hypothalamus; 3v=third ventricle; ME=median eminence; LH=lateral hypothalamus. BAM=binary alignment map

Figure S12: Expression of metabolism-associated receptors in the DVC magnaclasses

Violin plots of scaled expression of 10 genes (i.e. *Glp1r, Gfral, Calcr, Ramp3, Gipr, Lepr, Cckar, Cckbr ,Mc4r* and *Prlr*) coding for metabolism-associated receptors in the magnaclass1 and magnaclass2 neurons of the mouse DVC in fasted (magnaclass1 n=2,756; magnaclass2 n=2,789) and refed (magnaclass1 n=4,586; magnaclass2 n=4,423).

DVC=dorsal vagal complex

1578 Table S1: Murine brain databases used to map our unlabeled mouse dataset
1579 We used four databases included in the scRNAseq v2.16.0(*34, 37, 66, 67, 70*) R package and
1580 the celldex v1.12.0 built-in mouse RNA-seq reference (which we called 'SingleR' database)
1581 using SingleR (*69*) function to transfer labels to our dataset in R(*62*). The name, brain area and
1582 reference in which each database was made public are specified.
1583
1584 Table S2: Literature-derived markers per central nervous system cell identity
1585 We thoroughly searched in the literature for established markers at the mRNA and/or protein
1586 level. Some markers were found to be described for more than one cell population which are
1587 specified in columns 'notes' and 'notes_2'. After initial labeling of our murine dataset with the
1588 databases as described, we proceeded to obtain the average expression (on log-normalized
1589 counts) of each gene coding for the markers for the labeled cells (i.e. astrocyte, endothelial,
1590 microglia, neuron and oligodendrocyte) and unlabeled cells (i.e. unknown). We also calculated
1591 the average expression for each cluster in our dataset, established during our processing
1592 pipeline, at resolution 1.0.
1593
1594 Table S3: Literature-derived markers per central nervous system cell identity
1595 Breakdown of the cell identities (except neurons at layer 3 of cellular resolution) we established
1596 and corroborating using a combination of markers surveyed in **Table S2** and additional markers
1597 established using the FindConservedMarkers function from Seurat v5(*63*) package, indicating
1598 a cell state derived from the literature. For example, 's_fibroblasts' were named after finding
1599 high expression of *Stk39*, a stress-related marker(*35*).
1600
1601 Table S4: Expression of neurotransmitter-related genes in our murine neurons
1602 Expression of genes coding for neurotransmitter synthesis enzymes TH, DBH, TPH, GABA,
1603 NOS, prohormone SST and primary neurotransmitter transporters VMAT2, VGLUT1, VGLUT2,
1604 GLYT2 per neuron in our dataset. Expression and glutamate and GABA release are specified
1605 as binary variables (i.e. 0=no expression; 1=expression) in the green and blue columns,
1606 respectively. The percentile of the log-normalized expression is shown. ~55% of the neurons
1607 display expression of genes related to the synthesis/release of >1 primary neurotransmitter.
1608
1609 Table S5: Description of our DVC layer-3 neuronal cell identities established in mice
1610 Neurons were subset and reprocessed before labeling at layer-3 granularity. The MAST
1611 algorithm(*71*) was used through Seurat v5(*63*)on scaled data with a log fold-change threshold
1612 of 0.25 and detection threshold on ≥40% of cells on each neuronal cluster at resolution 1.0. We
1613 searched the resulting gene expression markers in the literature and compiled them. We then
1614 based the names for our cell identities on these genes.

1615

1616 Table S6: Expression of the murine DVC identity markers by rat DVC clusters

1617 Average log-normalized expression of the top 5 gene expression markers of each of our murine
1618 layer-3 cell identities (except duplicated genes n=37, and mouse specific genes n=27; total
1619 genes included=186) by rat DVC cluster at resolution 2.0.

1620

1621 Table S7: Description of our DVC layer-3 neuronal cell identities established in rats

1622 Rat neurons were subset and reprocessed before labeling at layers 2 and 3 of granularity. We
1623 used neuronal class gene expression markers to identify clusters at resolution 2.0 that
1624 belonged to each neuronal cell class. These cell classes were further subclustered and
1625 markers from Table S6 and UMAP projections were used to label each population in the
1626 dataset.

1627 Table S8: Genes with ≥2 log2 fold-change differential expression in neurons by magnaclass
1628 between meal-related treatments

1629 List of genes with a ≥2 log2 fold-change in magnaclass 1, magnaclass 2 or both
1630 magnaclasses neurons between meal-related treatments (i.e. refed versus ad libitum fed,
1631 and refed versus overnight fasted).

1632

1633 Table S9: Receptor expression in magnaclasses 1 and 2 between meal-related treatments in
1634 mice

1635 Differential expression analysis (MAST algorithm)(*71*) results for genes coding for metabolism
1636 related receptors between meal-related treatments (i.e. refed versus ad libitum fed, and refed
1637 versus overnight fasted) and per neuronal magnaclass. If a receptor is missing for any given
1638 comparison for any of the magnaclasses, the log fold-change of that gene between both
1639 treatments in that neuronal class was <0.1, therefore it is not reported (see **Methods**).

1640

1641 Table S10: Filtering of our and Dowsett datasets during processing

1642 Compilation of statistics and cells processed for the initial high quality cell filtering per sample.

1643

1644 Table S11: Cluster filtering of our and Dowsett datasets during processing

1645 Compilation of low quality cluster analysis statistics to filter high quality clusters per sample.

1646

1647 Table S12: Singlets retained per dataset after processing

1648 Number of doublets and singlets identified by DoubletFinder(*64*) after initial filtering of our and
1649 Dowset dataset per sample. Doublets were removed from the datasets before sample
1650 integration with Harmony(*65*) (this step was not performed in the rat dataset as it was only one
1651 sample, n=2 rat DVC).

1652

1653 Table S13: Labeled cells in our murine dataset

1654 Number of cell per treatment per identity layer 2.

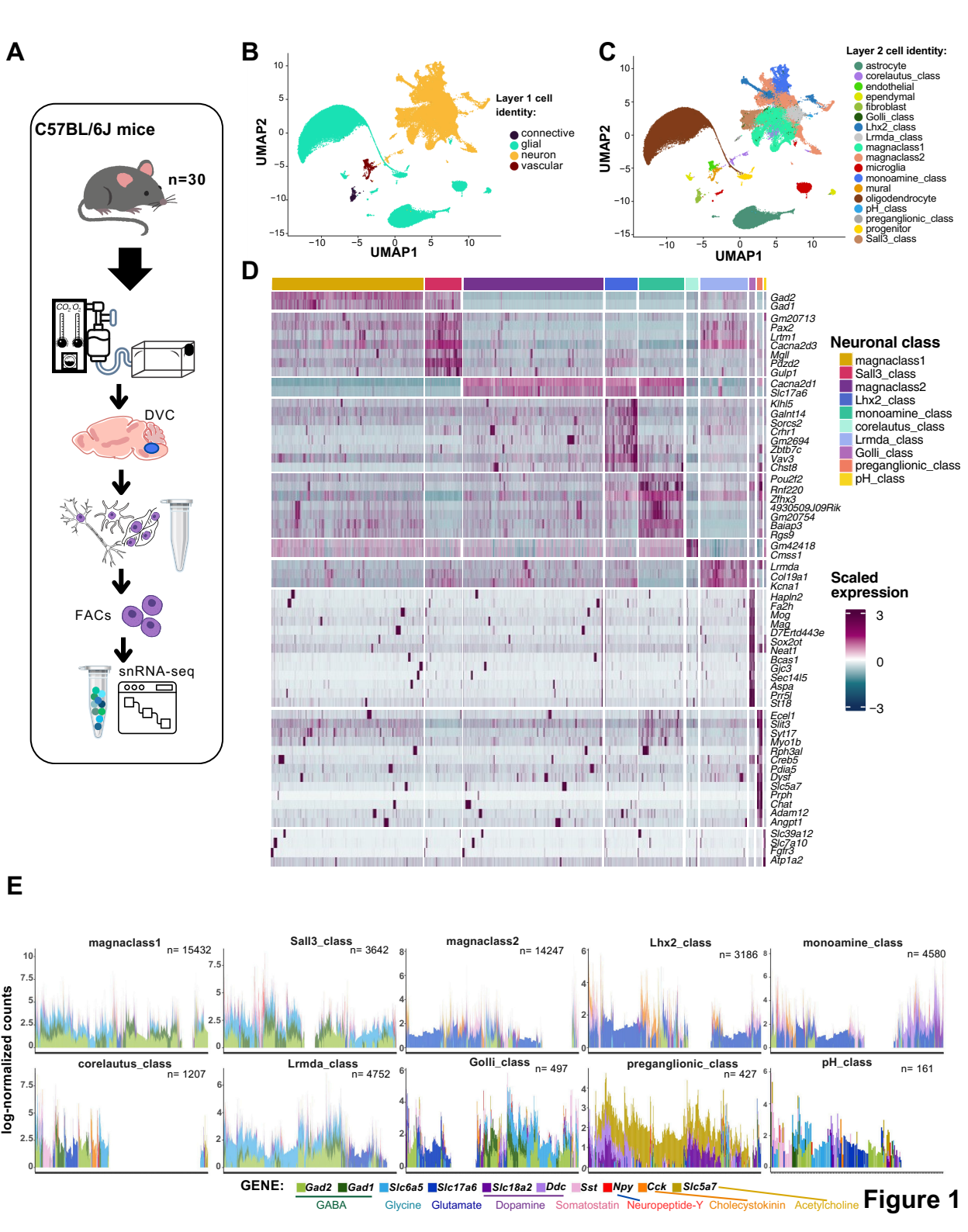
A
C57BL/6J mice
n=30
DVC
FACs
snRNA-seq
B
UMAP2
UMAP1
Layer 1 cell identity:
connective
glial
neuron
vascular
C
Layer 2 cell identity:
astrocyte
corelautus_class
endothelial
ependymal
fibroblast
Golli_class
Lhx2_class
Lrmda_class
magnaclass1
magnaclass2
microglia
monoamine_class
mural
oligodendrocyte
pH_class
preganglionic_class
progenitor
Sall3_class
D
Neuronal class
magnaclass1
Sall3_class
magnaclass2
Lhx2_class
monoamine_class
corelautus_class
Lrmda_class
Golli_class
preganglionic_class
pH_class
Scaled expression
Gad2
Gad1
Gm20713
Pax2
Lrtm1
Cacna2d3
Mgll
Pdzd2
Gulp1
Cacna2d1
Slc17a6
Klhl5
Galnt14
Sorcs2
Crhr1
Gm2694
Zbtb7c
Vav3
Chst8
Pou2f2
Rnf220
Zfhx3
4930509J09Rik
Gm20754
Baiap3
Rgs9
Gm42418
Cmss1
Lrmda
Col19a1
Kcna1
Hapln2
Fa2h
Mog
Mag
D7Ertd443e
Sox2ot
Neat1
Bcas1
Gjc3
Sec14l5
Aspa
Prrg1
St18
Ecel1
Slit3
Syt17
Myo1b
Rph3al
Creb5
Pdia5
Dyst
Slc5a7
Prph
Chat
Adam12
Angpt1
Slc39a12
Slc7a10
Fgfr3
Atp1a2
E
log-normalized counts
magnaclass1 n= 15432
Sall3_class n= 3642
magnaclass2 n= 14247
Lhx2_class n= 3186
monoamine_class n= 4580
corelautus_class n= 1207
Lrmda_class n= 4752
Golli_class n= 497
preganglionic_class n= 427
pH_class n= 161
GENE:
Gad2 Gad1 Slc6a5 Slc17a6 Slc18a2 Ddc Sst Npy Cck Slc5a7
GABA Glycine Glutamate Dopamine Somatostatin Neuropeptide-Y Cholecystokinin Acetylcholine

Figure 1

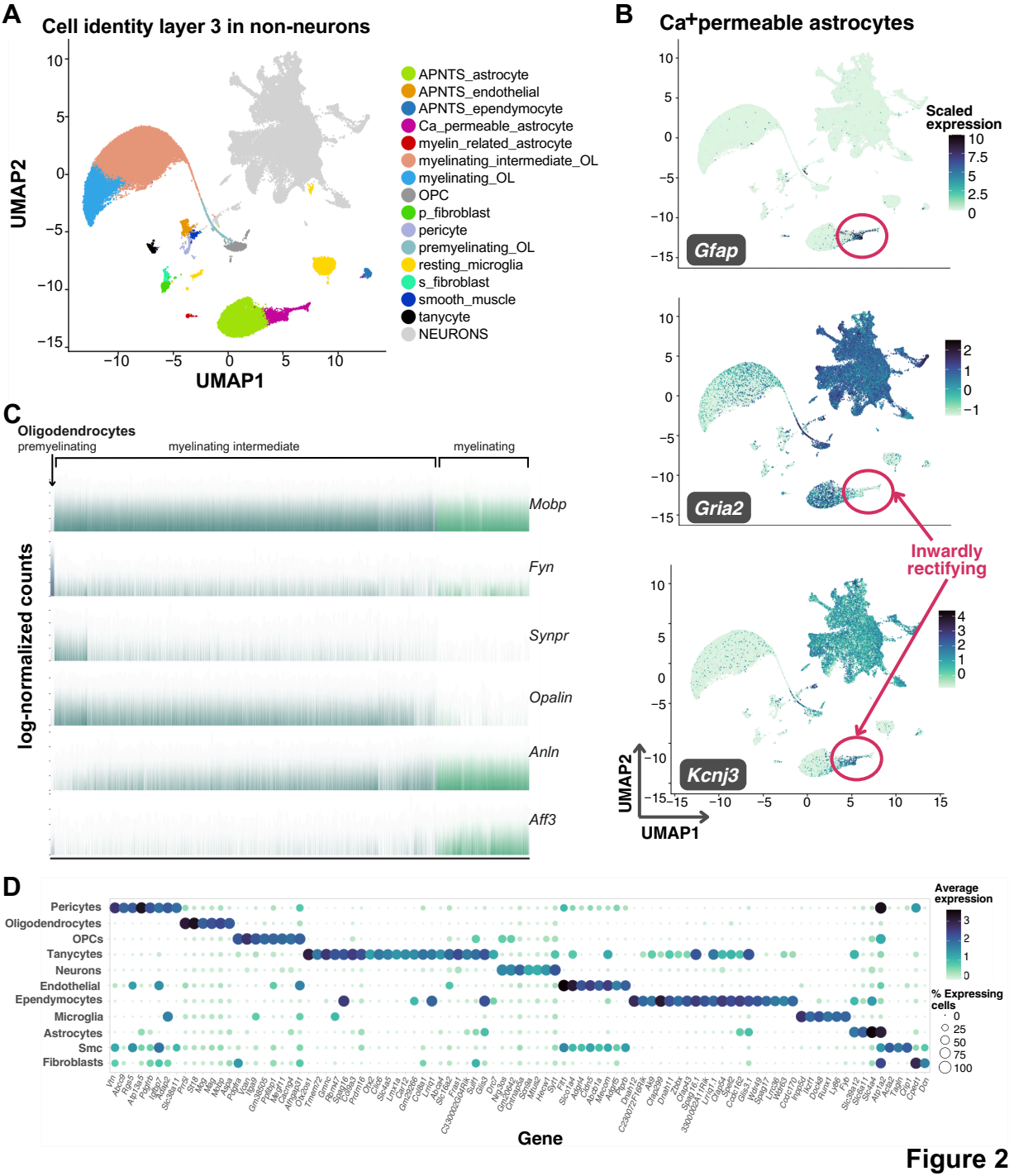
A
Cell identity layer 3 in non-neurons
UMAP2
UMAP1
APNTS_astrocyte
APNTS_endothelial
APNTS_ependymocyte
Ca_permeable_astrocyte
myelin_related_astrocyte
myelinating_intermediate_OL
myelinating_OL
OPC
p_fibroblast
pericyte
premyelinating_OL
resting_microglia
s_fibroblast
smooth_muscle
tanycyte
NEURONS
B
Ca+permeable astrocytes
Scaled expression
Gfap
Gria2
Kcnj3
Inwardly rectifying
UMAP2
UMAP1
C
Oligodendrocytes
premyelinating
myelinating intermediate
myelinating
log-normalized counts
Mobp
Fyn
Synpr
Opalin
Anln
Aff3
D
Pericytes
Oligodendrocytes
OPCs
Tanycytes
Neurons
Endothelial
Ependymocytes
Microglia
Astrocytes
Smc
Fibroblasts
Average expression
% Expressing cells
Gene

Figure 2

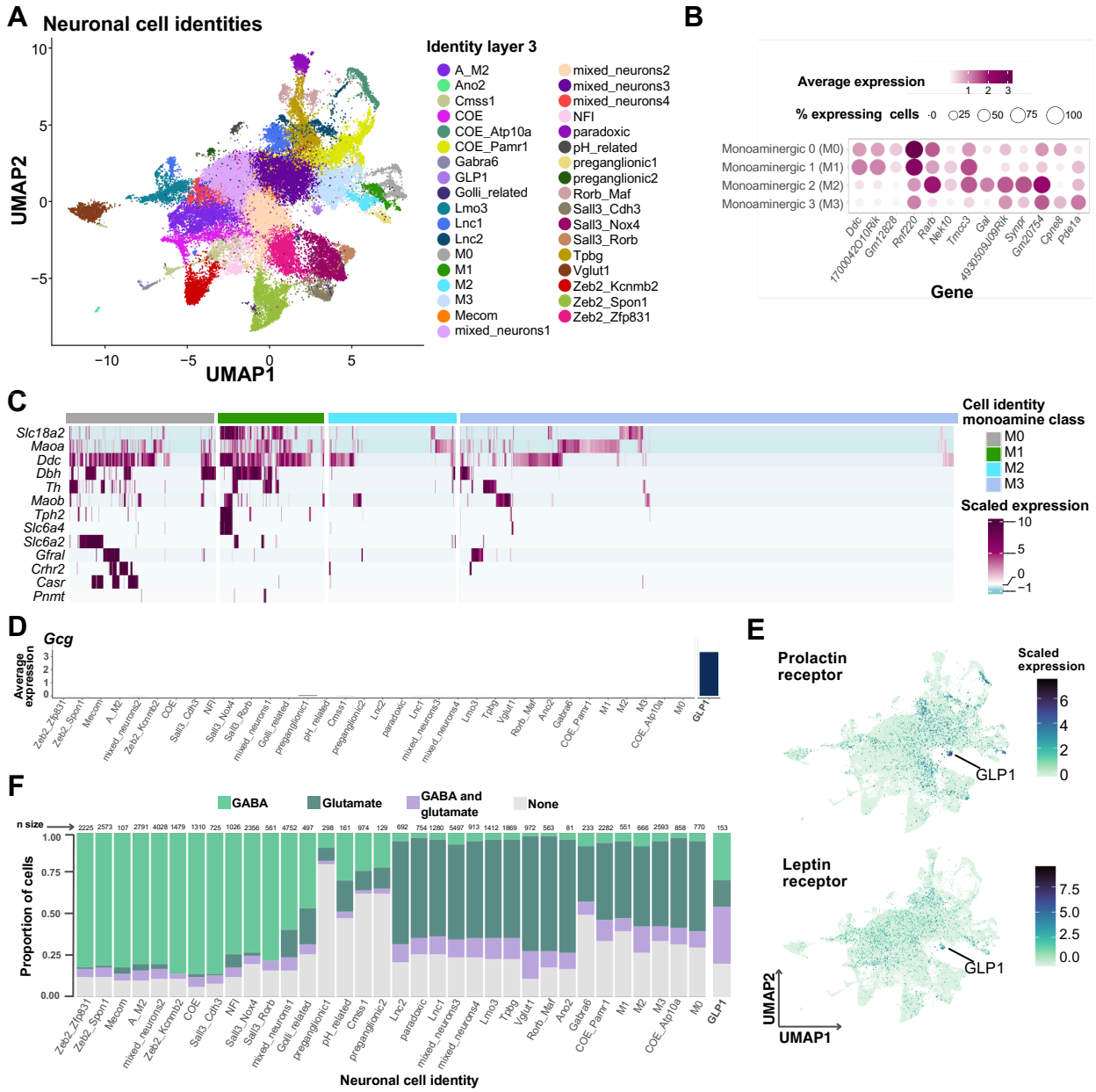
A
Neuronal cell identities
UMAP2
UMAP1
Identity layer 3
A_M2
Ano2
Cmss1
COE
COE_Atp10a
COE_Pamr1
Gabra6
GLP1
Golli_related
Lmo3
Lnc1
Lnc2
M0
M1
M2
M3
Mecom
mixed_neurons1
mixed_neurons2
mixed_neurons3
mixed_neurons4
NFI
paradoxic
pH_related
preganglionic1
preganglionic2
Rorb_Maf
Sall3_Cdh3
Sall3_Nox4
Sall3_Rorb
Tpbg
Vglut1
Zeb2_Kcnmb2
Zeb2_Spon1
Zeb2_Zfp831
B
Average expression
% expressing cells
Monoaminergic 0 (M0)
Monoaminergic 1 (M1)
Monoaminergic 2 (M2)
Monoaminergic 3 (M3)
Ddc
1700042O10Rik
Gm12828
Rnf220
Rarb
Nek10
Tmcc3
Gal
4930503J09Rik
Syngr
Gm20754
Cpne8
Pde1a
Gene
C
Slc18a2
Maoa
Ddc
Dbh
Th
Maob
Tph2
Slc6a4
Slc6a2
Gfral
Crhr2
Casr
Pnmt
Cell identity monoamine class
M0
M1
M2
M3
Scaled expression
D
Gcg
Average expression
E
Prolactin receptor
Leptin receptor
Scaled expression
GLP1
UMAP2
UMAP1
F
GABA
Glutamate
GABA and glutamate
None
n size
Proportion of cells
Neuronal cell identity

Figure 3

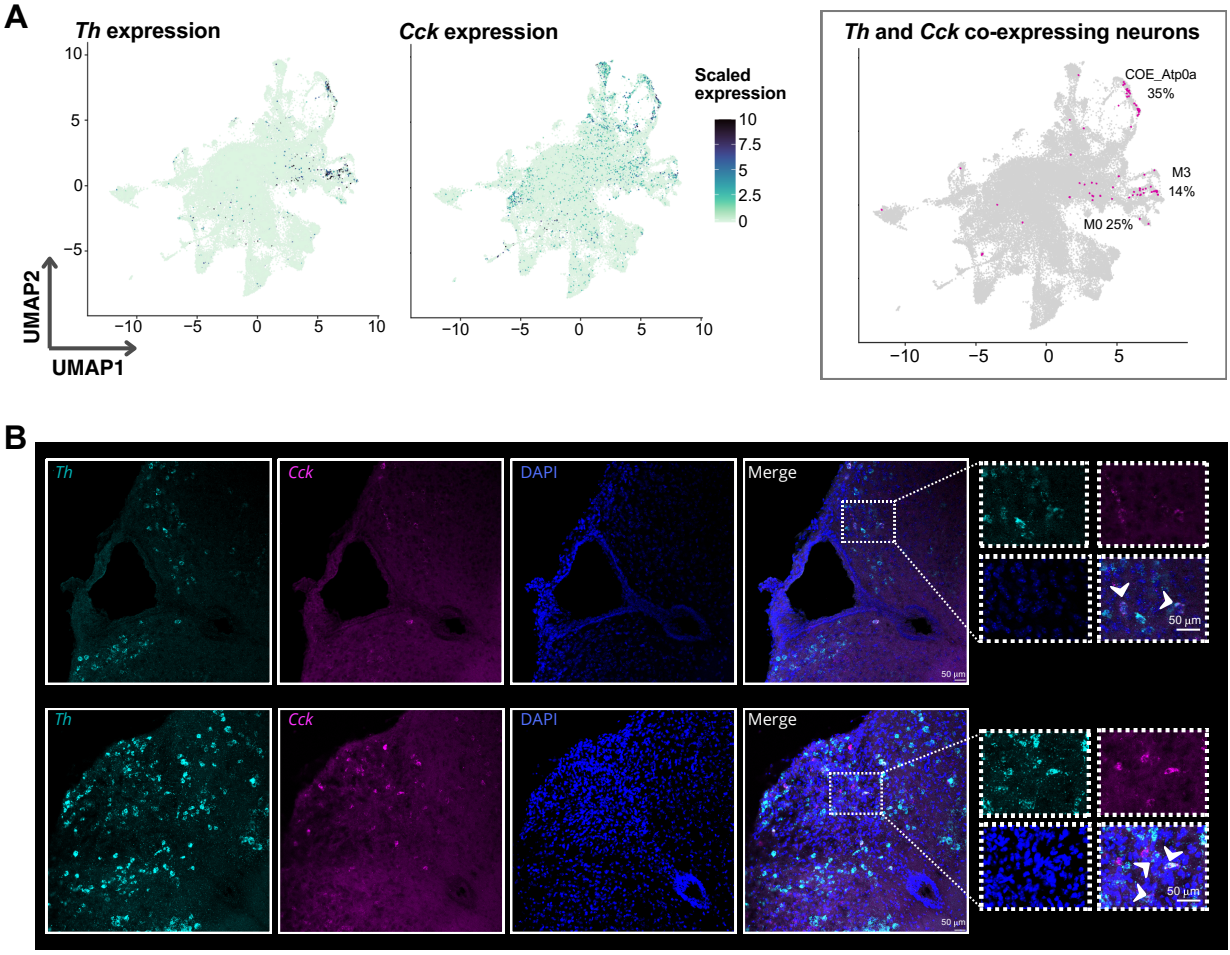
A
Th expression
Cck expression
Scaled expression
10
7.5
5
2.5
0
UMAP2
UMAP1
Th and Cck co-expressing neurons
COE_Atp0a
35%
M3
14%
M0 25%
B
Th
Cck
DAPI
Merge
50 µm

Figure 4

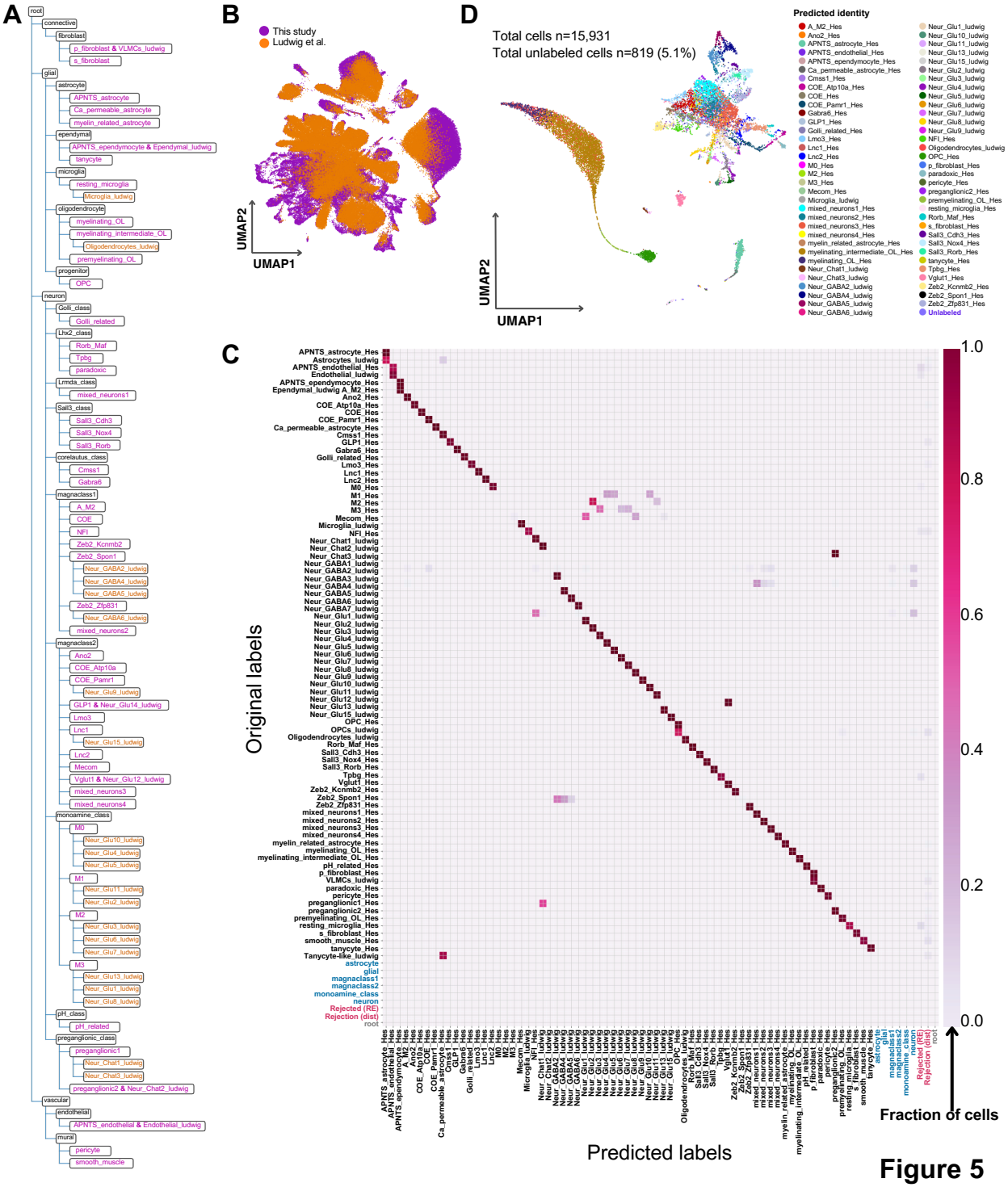
A
root
connective
fibroblast
p_fibroblast & VLMCs_ludwig
s_fibroblast
glial
astrocyte
APNTS_astrocyte
Ca_permeable_astrocyte
myelin_related_astrocyte
ependymal
APNTS_ependymocyte & Ependymal_ludwig
tanycyte
microglia
resting_microglia
Microglia_ludwig
oligodendrocyte
myelinating_OL
myelinating_intermediate_OL
Oligodendrocytes_ludwig
premyelinating_OL
progenitor
OPC
neuron
Golli_class
Golli_related
Lhx2_class
Rorb_Maf
Tpbg
paradoxic
Lrmda_class
mixed_neurons1
Sall3_class
Sall3_Cdh3
Sall3_Nox4
Sall3_Rorb
corelautus_class
Cmss1
Gabra6
magnaclass1
A_M2
COE
NFI
Zeb2_Kcnmb2
Zeb2_Spon1
Neur_GABA2_ludwig
Neur_GABA4_ludwig
Neur_GABA5_ludwig
Zeb2_Zfp831
Neur_GABA6_ludwig
mixed_neurons2
magnaclass2
Ano2
COE_Atp10a
COE_Pamr1
Neur_Glu9_ludwig
GLP1 & Neur_Glu14_ludwig
Lmo3
Lnc1
Neur_Glu15_ludwig
Lnc2
Mecom
Vglut1 & Neur_Glu12_ludwig
mixed_neurons3
mixed_neurons4
monoamine_class
M0
Neur_Glu10_ludwig
Neur_Glu4_ludwig
Neur_Glu5_ludwig
M1
Neur_Glu11_ludwig
Neur_Glu2_ludwig
M2
Neur_Glu3_ludwig
Neur_Glu6_ludwig
Neur_Glu7_ludwig
M3
Neur_Glu13_ludwig
Neur_Glu1_ludwig
Neur_Glu8_ludwig
pH_class
pH_related
preganglionic_class
preganglionic1
Neur_Chat1_ludwig
Neur_Chat3_ludwig
preganglionic2 & Neur_Chat2_ludwig
vascular
endothelial
APNTS_endothelial & Endothelial_ludwig
mural
pericyte
smooth_muscle
B
This study
Ludwig et al.
UMAP2
UMAP1
D
Total cells n=15,931
Total unlabeled cells n=819 (5.1%)
UMAP2
UMAP1
Predicted identity
A_M2_Hes
Ano2_Hes
APNTS_astrocyte_Hes
APNTS_endothelial_Hes
APNTS_ependymocyte_Hes
Ca_permeable_astrocyte_Hes
Cmss1_Hes
COE_Atp10a_Hes
COE_Hes
COE_Pamr1_Hes
Gabra6_Hes
GLP1_Hes
Golli_related_Hes
Lmo3_Hes
Lnc1_Hes
Lnc2_Hes
M0_Hes
M1_Hes
M2_Hes
M3_Hes
Mecom_Hes
Microglia_ludwig
mixed_neurons1_Hes
mixed_neurons2_Hes
mixed_neurons3_Hes
mixed_neurons4_Hes
myelin_related_astrocyte_Hes
myelinating_intermediate_OL_Hes
myelinating_OL_Hes
Neur_Chat1_ludwig
Neur_Chat3_ludwig
Neur_GABA2_ludwig
Neur_GABA4_ludwig
Neur_GABA5_ludwig
Neur_GABA6_ludwig
Neur_Glu1_ludwig
Neur_Glu2_ludwig
Neur_Glu3_ludwig
Neur_Glu4_ludwig
Neur_Glu5_ludwig
Neur_Glu6_ludwig
Neur_Glu7_ludwig
Neur_Glu8_ludwig
Neur_Glu9_ludwig
NFI_Hes
Oligodendrocytes_ludwig
OPC_Hes
p_fibroblast_Hes
paradoxic_Hes
pericyte_Hes
preganglionic2_Hes
premyelinating_OL_Hes
resting_microglia_Hes
Rorb_Maf_Hes
s_fibroblast_Hes
Sall3_Cdh3_Hes
Sall3_Nox4_Hes
Sall3_Rorb_Hes
tanycyte_Hes
Tpbg_Hes
Vglut1_Hes
Zeb2_Kcnmb2_Hes
Zeb2_Spon1_Hes
Zeb2_Zfp831_Hes
Unlabeled
C
Original labels
Predicted labels
Fraction of cells
1.0
0.8
0.6
0.4
0.2
0.0

Figure 5

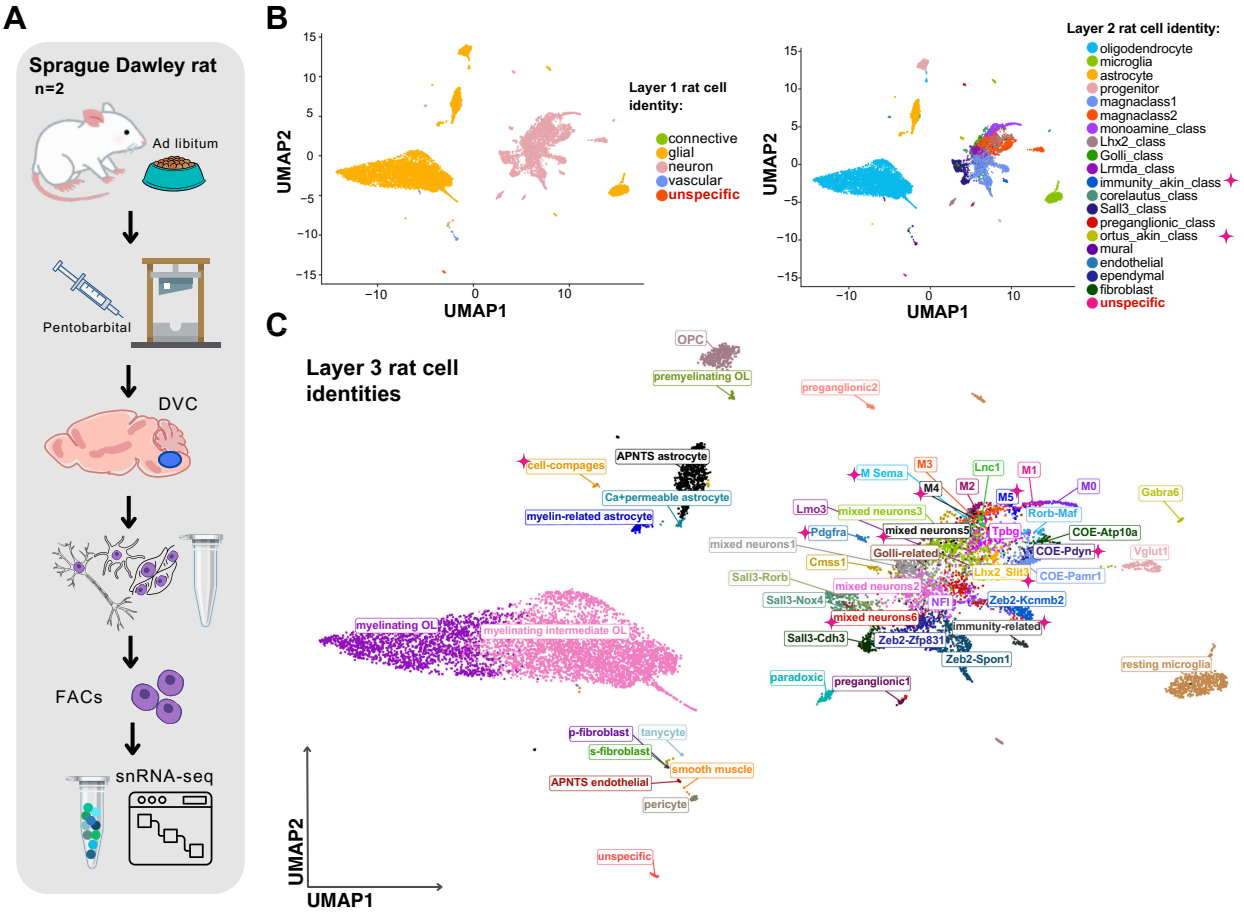
A
Sprague Dawley rat
n=2
Ad libitum
Pentobarbital
DVC
FACs
snRNA-seq
B
UMAP2
UMAP1
Layer 1 rat cell identity:
connective
glial
neuron
vascular
unspecific
Layer 2 rat cell identity:
oligodendrocyte
microglia
astrocyte
progenitor
magnaclass1
magnaclass2
monoamine_class
Lhx2_class
Golli_class
Lrmda_class
immunity_akin_class
corelautus_class
Sall3_class
preganglionic_class
ortus_akin_class
mural
endothelial
ependymal
fibroblast
unspecific
C
Layer 3 rat cell identities
OPC
premyelinating OL
preganglionic2
cell-compages
APNTS astrocyte
Ca+permeable astrocyte
myelin-related astrocyte
M Sema
M3
Lnc1
M1
M4
M2
M5
M0
Gabra6
Lmo3
mixed neurons3
Rorb-Maf
Pdgfra
mixed neurons5
Tpbg
COE-Atp10a
mixed neurons1
Golli-related
COE-Pdyn
Vglut1
Cmss1
Lhx2_Slit3
COE-Pamr1
Sall3-Rorb
mixed neurons2
Sall3-Nox4
NFI
Zeb2-Kcnmb2
mixed neurons6
immunity-related
Sall3-Cdh3
Zeb2-Zfp831
Zeb2-Spon1
resting microglia
paradoxic
preganglionic1
myelinating OL
myelinating intermediate OL
p-fibroblast
tanycyte
s-fibroblast
smooth muscle
APNTS endothelial
pericyte
unspecific
UMAP2
UMAP1

Figure 6

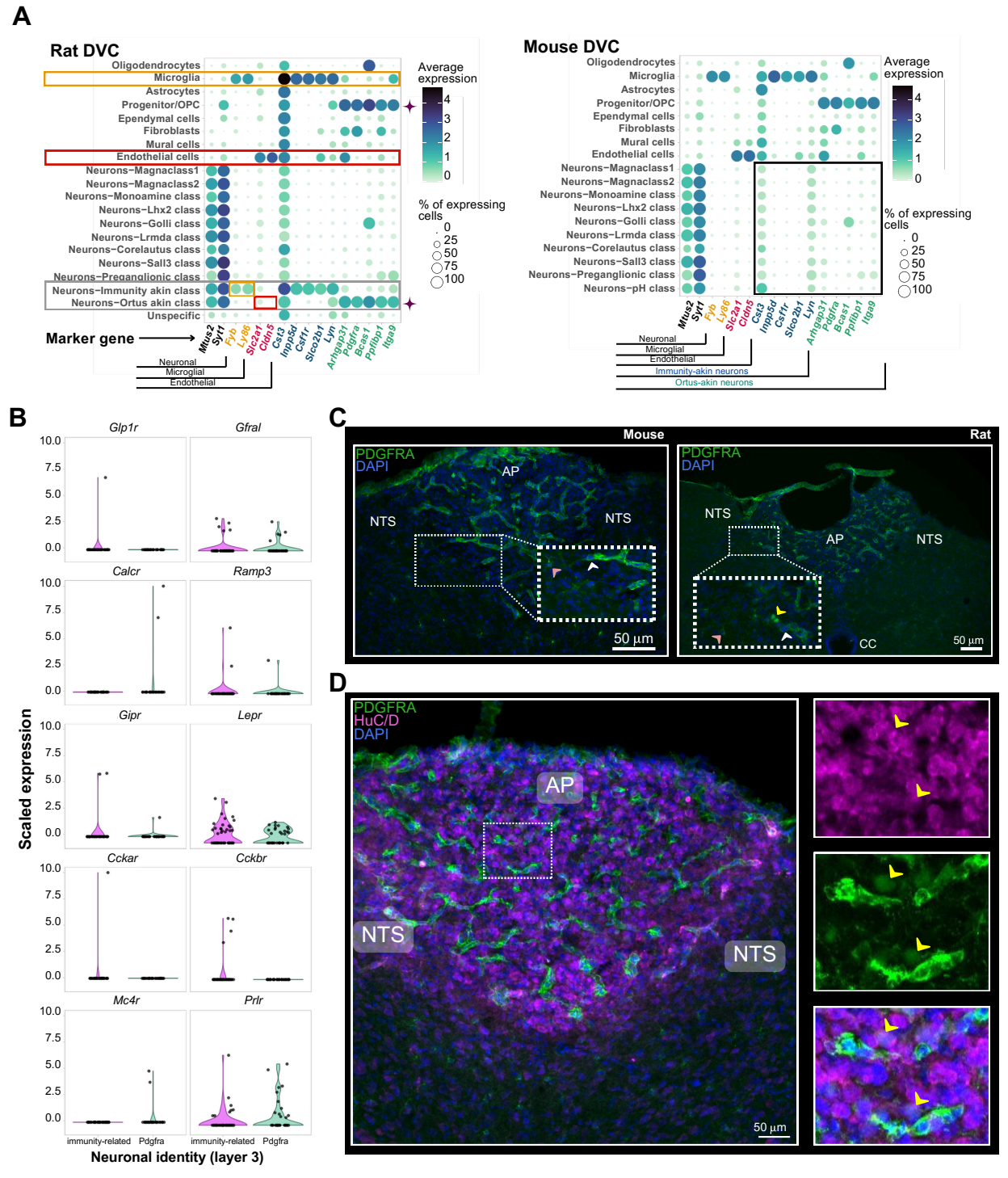
A
Rat DVC
Mouse DVC
Oligodendrocytes
Microglia
Astrocytes
Progenitor/OPC
Ependymal cells
Fibroblasts
Mural cells
Endothelial cells
Neurons−Magnaclass1
Neurons−Magnaclass2
Neurons−Monoamine class
Neurons−Lhx2 class
Neurons−Golli class
Neurons−Lrmda class
Neurons−Corelautus class
Neurons−Sall3 class
Neurons−Preganglionic class
Neurons−Immunity akin class
Neurons−Ortus akin class
Neurons−pH class
Unspecific
Average expression
% of expressing cells
Marker gene
Mtus2
Syt1
Fyb
Lyl6
Slc2a1
Cldn5
Cst3
Inpp5d
Csf1r
Slco2b1
Lyn
Arhgap31
Pdgfra
Bcas1
Ppfibp1
Itga9
Neuronal
Microglial
Endothelial
Immunity-akin neurons
Ortus-akin neurons
B
Glp1r
Gfral
Calcr
Ramp3
Gipr
Lepr
Cckar
Cckbr
Mc4r
Prlr
Scaled expression
immunity-related
Pdgfra
Neuronal identity (layer 3)
C
Mouse
Rat
PDGFRA
DAPI
AP
NTS
CC
50 µm
D
HuC/D

Figure 7

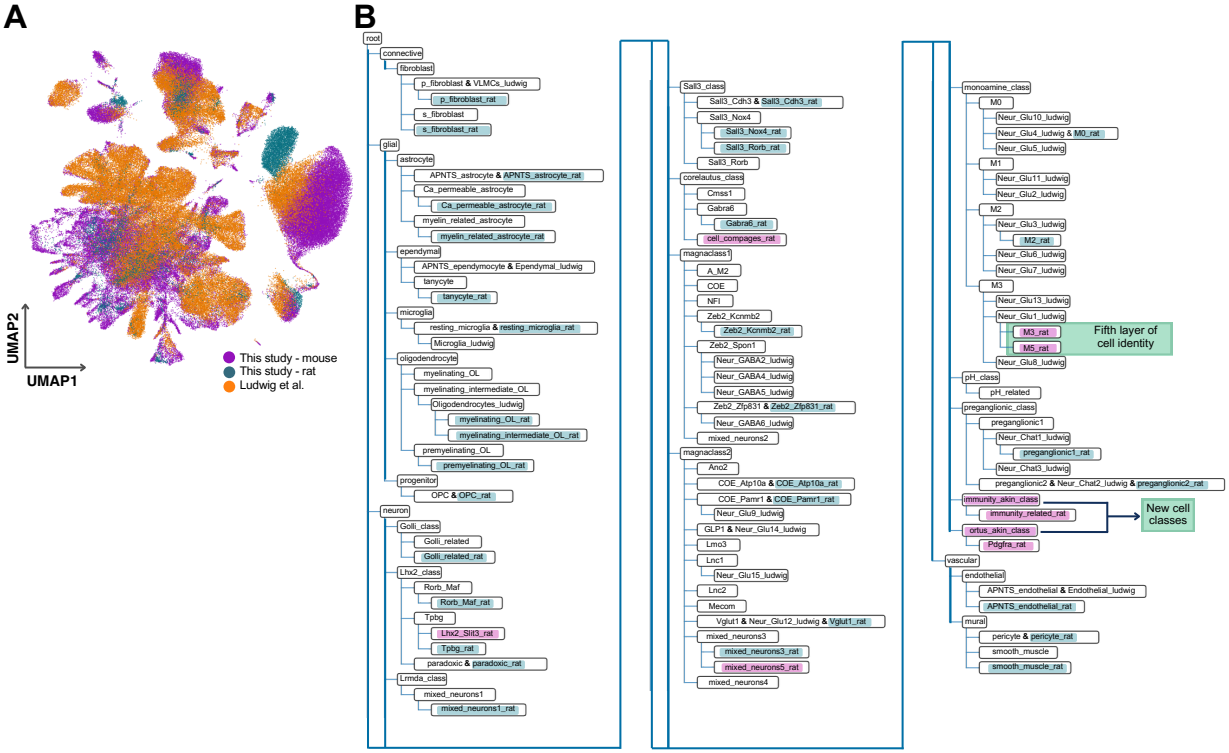
A
UMAP2
UMAP1
This study - mouse
This study - rat
Ludwig et al.
B
root
connective
fibroblast
p_fibroblast & VLMCs_ludwig
p_fibroblast_rat
s_fibroblast
s_fibroblast_rat
glial
astrocyte
APNTS_astrocyte & APNTS_astrocyte_rat
Ca_permeable_astrocyte
Ca_permeable_astrocyte_rat
myelin_related_astrocyte
myelin_related_astrocyte_rat
ependymal
APNTS_ependymocyte & Ependymal_ludwig
tanycyte
tanycyte_rat
microglia
resting_microglia & resting_microglia_rat
Microglia_ludwig
oligodendrocyte
myelinating_OL
myelinating_intermediate_OL
Oligodendrocytes_ludwig
myelinating_OL_rat
myelinating_intermediate_OL_rat
premyelinating_OL
premyelinating_OL_rat
progenitor
OPC & OPC_rat
neuron
Golli_class
Golli_related
Golli_related_rat
Lhx2_class
Rorb_Maf
Rorb_Maf_rat
Tpbg
Lhx2_Sitl3_rat
Tpbg_rat
paradoxic & paradoxic_rat
Lrmda_class
mixed_neurons1
mixed_neurons1_rat
Sall3_class
Sall3_Cdh3 & Sall3_Cdh3_rat
Sall3_Nox4
Sall3_Nox4_rat
Sall3_Rorb_rat
Sall3_Rorb
corelautus_class
Cmss1
Gabra6
Gabra6_rat
cell_compages_rat
magnaclass1
A_M2
COE
NF1
Zeb2_Kcnmb2
Zeb2_Kcnmb2_rat
Zeb2_Spon1
Neur_GABA2_ludwig
Neur_GABA4_ludwig
Neur_GABA5_ludwig
Zeb2_Zfp831 & Zeb2_Zfp831_rat
Neur_GABA6_ludwig
mixed_neurons2
magnaclass2
Anc2
COE_Atp10a & COE_Atp10a_rat
COE_Pamr1 & COE_Pamr1_rat
Neur_Glu9_ludwig
GLP1 & Neur_Glu14_ludwig
Lmo3
Lnc1
Neur_Glu15_ludwig
Lnc2
Mecom
Vglut1 & Neur_Glu12_ludwig & Vglut1_rat
mixed_neurons3
mixed_neurons3_rat
mixed_neurons5_rat
mixed_neurons4
monoamine_class
M0
Neur_Glu10_ludwig
Neur_Glu4_ludwig & M0_rat
Neur_Glu5_ludwig
M1
Neur_Glu11_ludwig
Neur_Glu2_ludwig
M2
Neur_Glu3_ludwig
M2_rat
Neur_Glu6_ludwig
Neur_Glu7_ludwig
M3
Neur_Glu13_ludwig
Neur_Glu1_ludwig
M3_rat
M5_rat
Fifth layer of cell identity
Neur_Glu8_ludwig
pH_class
pH_related
preganglionic_class
preganglionic1
Neur_Chat1_ludwig
preganglionic1_rat
Neur_Chat3_ludwig
preganglionic2 & Neur_Chat2_ludwig & preganglionic2_rat
immunity_akin_class
immunity_related_rat
ortus_akin_class
Pdgfra_rat
New cell classes
vascular
endothelial
APNTS_endothelial & Endothelial_ludwig
APNTS_endothelial_rat
mural
pericyte & pericyte_rat
smooth_muscle
smooth_muscle_rat

Figure 8

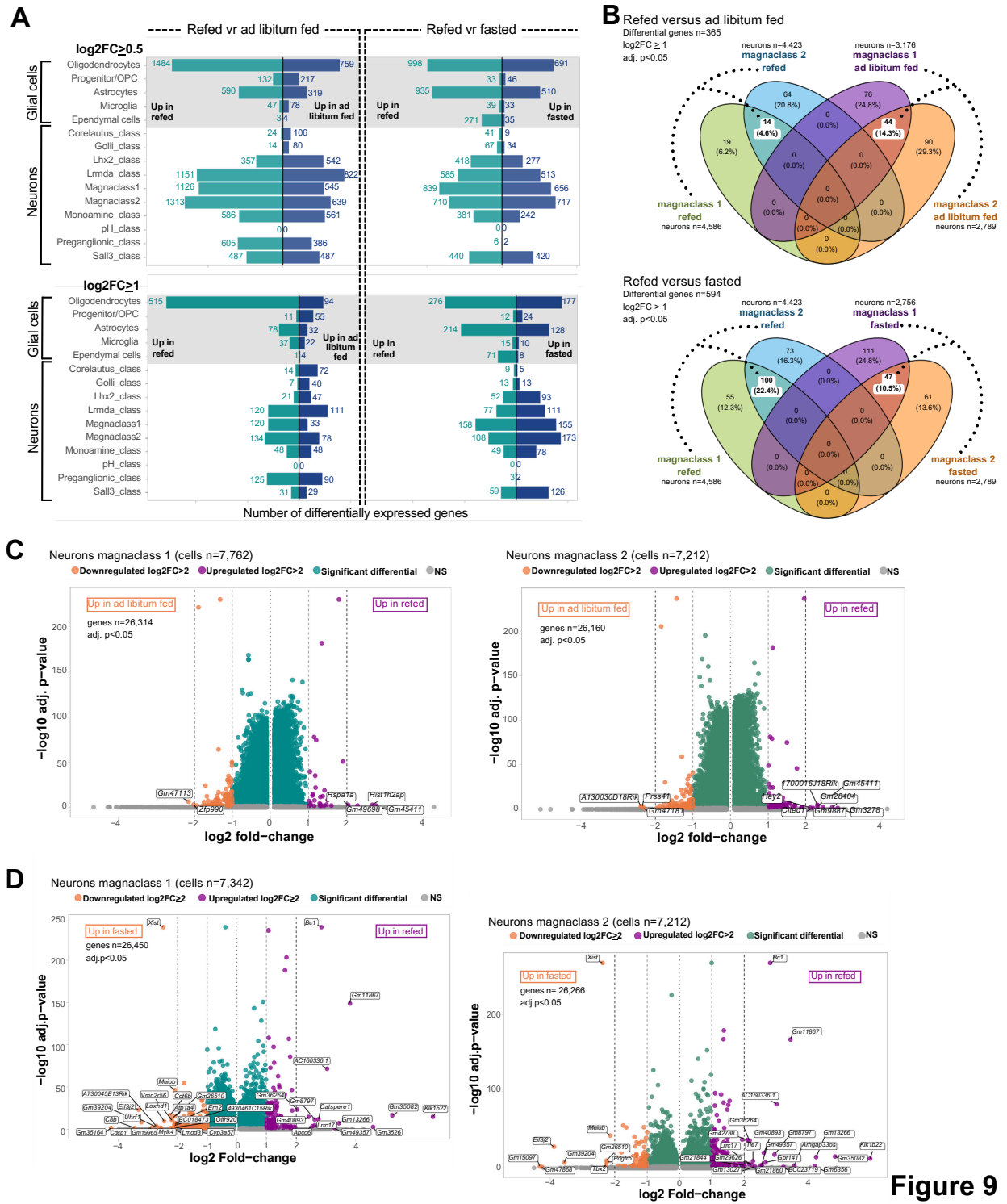
A
Refed vr ad libitum fed
Refed vr fasted
log2FC≥0.5
Glial cells
Neurons
Oligodendrocytes
Progenitor/OPC
Astrocytes
Microglia
Ependymal cells
Corelautus_class
Golli_class
Lhx2_class
Lrmda_class
Magnaclass1
Magnaclass2
Monoamine_class
pH_class
Preganglionic_class
Sall3_class
Up in refed
Up in ad libitum fed
Up in refed
Up in fasted
log2FC≥1
Up in refed
Up in ad libitum fed
Up in refed
Up in fasted
Number of differentially expressed genes
B
Refed versus ad libitum fed
Differential genes n=365
log2FC ≥ 1
adj. p<0.05
neurons n=4,423
magnaclass 2
refed
neurons n=3,176
magnaclass 1
ad libitum fed
magnaclass 1
refed
neurons n=4,586
magnaclass 2
ad libitum fed
neurons n=2,789
Refed versus fasted
Differential genes n=594
log2FC ≥ 1
adj. p<0.05
neurons n=4,423
magnaclass 2
refed
neurons n=2,756
magnaclass 1
fasted
magnaclass 1
refed
neurons n=4,586
magnaclass 2
fasted
neurons n=2,789
C
Neurons magnaclass 1 (cells n=7,762)
Downregulated log2FC≥2
Upregulated log2FC≥2
Significant differential
NS
Up in ad libitum fed
genes n=26,314
adj. p<0.05
Up in refed
−log10 adj. p−value
log2 fold−change
Neurons magnaclass 2 (cells n=7,212)
Up in ad libitum fed
genes n=26,160
adj. p<0.05
Up in refed
D
Neurons magnaclass 1 (cells n=7,342)
Up in fasted
genes n=26,450
adj.p<0.05
Up in refed
−log10 adj.p−value
log2 Fold−change
Neurons magnaclass 2 (cells n=7,212)
Up in fasted
genes n= 26,266
adj.p<0.05
Up in refed
−log10 adj.p−value
log2 Fold−change

Figure 9